A&A 578, A95 (2015)
DOI: 10.1051/0004-6361/201425175

Astronomy & Astrophysics

Neutral carbon and CO in 76 (U)LIRGs and starburst galaxy centers

A method to determine molecular gas properties in luminous galaxies

F. P. Israel, M. J. F. Rosenberg, and P. van der Werf

Sterrewacht Leiden, Leiden University, PO Box 9513, 2300 RA Leiden, The Netherlands
e-mail: israel@strw.leidenuniv.nl

Received 17 October 2014 / Accepted 30 March 2015

ABSTRACT

In this paper we present fluxes in the [C I] lines of neutral carbon at the centers of some 76 galaxies with far-infrared luminosities ranging from 10^9 to 10^{12} $L_\odot$, as obtained with the *Herschel* Space Observatory and ground-based facilities, along with the line fluxes of the $J = 7-6$, $J = 4-3$, $J = 2-1$ ^{12}CO, and $J = 2-1$ ^{13}CO transitions. With this dataset, we determine the behavior of the observed lines with respect to each other and then investigate whether they can be used to characterize the molecular interstellar medium (ISM) of the parent galaxies in simple ways and how the molecular gas properties define the model results. In most starburst galaxies, the [C I] to ^{13}CO line flux ratio is much higher than in Galactic star-forming regions, and it is correlated to the total far-infrared luminosity. The [C I] (1−0)/ ^{12}CO (4−3), the [C I] (2−1)/ ^{12}CO (7−6), and the [C I] (2−1)/(1−0) flux ratios are correlated, and they trace the excitation of the molecular gas. In the most luminous infrared galaxies (LIRGs), the ISM is fully dominated by dense ($n(\mathrm{H_2}) = 10^4-10^5$ cm^{-3}) and moderately warm ($T_{\rm kin} \approx 30$ K) gas clouds that appear to have low [C°]/[CO] and [^{13}CO]/[^{12}CO] abundances. In less luminous galaxies, emission from gas clouds at lower densities becomes progressively more important, and a multiple-phase analysis is required to determine consistent physical characteristics. Neither the ^{12}CO nor the [C I] velocity-integrated line fluxes are good predictors of molecular hydrogen column densities in individual galaxies. In particular, so-called X([C I]) conversion factors are not superior to $X(^{12}\mathrm{CO})$ factors. The methods and diagnostic diagrams outlined in this paper also provide a new and relatively straightforward means of deriving the physical characteristics of molecular gas in high-redshift galaxies up to $z = 5$, which are otherwise hard to determine.

Key words. surveys – ISM: abundances – galaxies: ISM – galaxies: starburst – galaxies: nuclei – ISM: molecules

1. Introduction

Carbon monoxide (CO), the molecular species most commonly observed in galaxies, is widely used as a tracer for molecular hydrogen (H_2). Molecular hydrogen accounts for the bulk of the molecular gas and is a major component of the interstellar medium (ISM) in galaxies, but is much harder to observe. When shielding is reduced (low metallicity) and radiation enhanced (starburst), CO is readily photodissociated into its constituent parts, carbon (C) and oxygen (O). As the ionization potential of neutral carbon, (C°) is close to the dissociation energy of CO, and it can only exist in a narrow range of physical conditions. This is clearly shown by a variety of ISM models, for instance, those of Meijerink et al. (2007).

The CO and neutral carbon [C I] submillimeter lines are the major coolants for most of the dense molecular gas from which stars are thought to form. Ground-based observations of [C I] emission can be performed from a few dry sites at high elevation, at least in the [C I] (1−0) line, i.e., the $^3P_1-^3P_0$ [CI] transition at 492 GHz. This is much less practical for observations of the $^3P_2-^3P_1$ [CI] line at 809 GHz, hereafter designated as [C I] (2−1). Like the higher J transitions of CO, the [C I] lines are best observed from an airborne platform (such as SOFIA), or from a platform in space (such as the now defunct *Herschel* Space Observatory).

Until the *Herschel* space mission, the number of published extragalactic [C I] observations was limited. Beyond the Local Group, the [C I] 492 GHz line was surveyed in two dozen galaxies by Gerin & Phillips (2000) and by Israel & Baas (2002), and mapped in a few bright northern galaxies (see Israel et al. 2009b, and references therein). Gerin & Phillips found that, relative to the low-J ^{12}CO lines, [C I] (1−0) is weaker in galaxy nuclei but stronger in disks, particularly outside star-forming regions. Israel & Baas compared the [C I] (1−0) with the $J = 2-1$ ^{13}CO and $J = 4-3$ ^{12}CO lines. They find that in galaxy centers, the [C I] (1−0) brightness temperature is close to or slightly lower than that of the adjacent ^{12}CO $J = 4-3$ line, but significantly higher than the $J = 2-1$ ^{13}CO brightness temperature. This is very different from the situation pertaining to Galactic photon-dominated regions (PDRs), where the [C I] brightness temperatures are invariably much lower, both as predicted by models (Kaufman et al. 1999) and as observed in actual fact (Plume et al. 1999; Tatematsu et al. 1999). Israel & Baas also find that the [C I] (1−0)/ ^{13}CO (2−1) temperature ratio increases with the [C I] luminosity in the same beam. They use radiative transfer models to show that the C° abundance usually exceeds that of the CO. Both groups concluded that the [CI] emission arises from a warm and moderately dense ($n = 10^3-10^4$ cm^{-3}) gas.

With the mission of the *Herschel* Space Observatory, more measurements of galaxies in both [CI] lines have become available. Some of these have already been published, and others are presented here for the first time. Table 1 lists the sample of galaxies in which at least one [C I] line has been measured, which will be discussed in this paper. Positions, radial velocities, and distances[1] were taken from the NASA-IPAC Extragalactic Database (NED), and the logarithmic far-infrared (FIR) fluxes

[1] Cosmology-corrected luminosity distances assuming $H_0 = 73.0$ km s^{-1} Mpc, $\omega_{\rm m} = 0.27$, $\omega_{\rm vac} = 0.73$, corrected to the reference frame defined by the 3 K microwave background.

Table 1. Galaxy sample.

Name	RA(2000)[a] (h m s)	Dec(2000)[a] (d m s)	V_{LSR}[a] (km s^{-1})	D[a] (Mpc)	lg FIR[b] (W m^{-2})	lg L_{FIR} ($L_{\odot}$)	Table[a]
NGC 34	00 11 06.5	−12 06 26	5881	79.3	−12.12	11.21	2
IC10	00 20 17.3	+59 18 14	−348	0.85	−11.72	7.62	5
NGC 253	00 47 33.1	−25 17 18	243	3.4	−10.42	10.15	2, 5
NGC 278	00 52 04.3	+47 33 02	840	11.3	−11.87	9.76	5
MGC+12-02-001	00 54 03.6	+73 05 12	4706	66.1	−11.77	12.35	2
IC 1623(Arp 236)	01 07 47.2	−17 30 25	6016	80.7	−11.97	11.37	2
NGC 660	01 43 02.4	+13 38 42	910	12.2	−11.46	10.26	5
NGC 891	02 22 33.4	+42 20 57	528	9.4	−11.53	9.89	5
Maffei 2	02 41 55.0	+59 36 15	189	3.1	−11.23	9.11	5
NGC 1068/M77	02 42 40.7	−00 00 48	1010	15.2	−11.04	10.75	4.5
NGC 1056	02 42 48.3	+28 34 27	1545	21.4	−12.49	10.00	4
NGC 1275 (Per A)	03 19 48.1	+41 30 42	5264	70.9	−12.47	10.71	3
NGC 1365	03 33 36.4	−36 08 25	1636	21.5	−11.36	10.86	2
IC 342	03 46 48.5	+68 05 47	126	3.5	−11.36	8.60	5
NGC1482	03 54 38.9	−20 30 10	1916	25.4	−11.79	10.50	3
NGC 1614	04 33 59.8	−08 34 44	4778	64.2	−11.82	11.33	2
IRAS F05189-2524	05 21 01.4	−25 21 45	12760	173	−12.22	11.78	2
NGC 2146	06 18 37.7	+78 21 25	893	16.7	−11.16	10.53	2
Henize 2-10	08 36 15.1	−26 24 34	873	10.4	−11.95	9.56	5
NGC 2623 (Arp 243)	08 38 24.1	+25 45 17	5549	79.4	−11.94	11.34	2
NGC 2798	09 17 22.8	+41 59 59	1725	28.6	−11.96	10.43	3
IRAS 09022-3615	09 04 12.7	−36 27 01	17880	248	−12.29	11.98	4
UGC 05101	09 35 51.6	+61 21 11	1802	164	−12.19	11.71	4
NGC 3034/M 82	09 55 52.7	+69 40 46	228	3.3	−10.28	10.23	5
NGC 3079	10 01 57.8	+55 40 47	1260	20.7	−11.60	10.38	5
NGC 3227	10 23 30.6	+19 51 54	1157	20.3	−12.32	9.48	4
NGC 3256	10 27 51.3	−43 54 13	2804	37.0	−11.34	11.34	2
NGC 3521	11 05 48.6	−00 02 09	801	8.0	−11.71	9.57	3
NGC 3627/M66	11 20 14.9	+12 59 30	727	6.5	−11.61	9.50	3
NGC 3628	11 20 17.0	+13 35 23	469	8.5	−11.54	9.59	5
Arp 299/IC 694/NGC 3690	11 28 31.0	+58 33 41	3089	49.1	−11.32	11.45	2
ESO320-G030	11 53 11.7	−39 07 49	3232	39.2	−11.78	11.03	2
NGC 3982	11 56 28.1	+55 07 31	1109	21.0	−12.37	9.73	4
NGC 4038	12 01 53.0	−18 52 03	1642	23.3	−11.65	10.57	4, 5
NGC 4039	12 01 53.5	−18 53 10	1642	23.3	−11.65	10.57	4
NGC 4051	12 03 09.6	+44 31 53	700	12.9	−12.27	9.53	4
NGC 4151	12 10 32.6	+39 24 21	995	20.0	−12.51	9.15	4
NGC 4254/M99	12 18 49.6	+14 24 59	2407	39.8	−11.78	10.90	3
NGC 4321/M100	12 22 54.8	+15 49 19	1571	14.1	−11.88	9.90	3
NGC 4388	12 25 46.7	+12 39 44	2524	41.4	−12.24	9.76	4
NGC 4418	12 26 54.6	−00 52 39	2179	34.7	−11.73	10.83	2
IC 3639	12 40 52.8	−36 45 21	3275	35.3	−12.23	10.51	4
NGC 4536	12 34 27.0	+02 11 17	1808	30.8	−11.81	10.64	3
NGC 4631	12 42 08.0	+32 32 29	806	7.6	−11.50	9.74	3
NGC 4736/M94	12 50 53.0	+41 07 15	308	4.83	−11.50	9.35	3, 5
Mrk 231/7Zw490	12 56 14.2	+56 52 25	12642	178	−11.8	12.19	2, 5
NGC 4826/M64	12 56 43.6	+21 40 59	357	3.8	−11.66	9.23	3, 5
NGC 4945	13 05 27.5	−49 28 06	555	4.3	−10.67	9.94	3, 5
IRAS 13120-5453	13 15 06.3	−55 09 23	9222	134	−11.71	12.01	2
NGC 5055/M63	13 15 49.3	+42 01 45	484	8.3	−11.66	9.66	3
Arp 193/IC 883	13 20 35.3	+34 08 22	6985	103	−12.10	11.38	2
NGC 5128/Cen A	13 25 27.6	−43 01 09	269	3.8	−11.01	9.62	4, 5
NGC 5135	13 25 44.0	−29 50 01	4105	57.7	−12.04	10.97	2
ESO 173-G015	13 27 23.8	−57 29 22	2918	32.4	−11.44	11.28	2
NGC 5194/M51	13 29 52.7	+47 11 43	672	9.1	−11.59	10.85	3,5
NGC 5236/M83	13 37 00.9	−29 51 56	245	4.0	−11.22	9.34	4, 5
Mrk 273/1Zw71	13 44 42.1	+55 53 13	11326	162	−11.9	12.00	2
Circinus	14 13 09.9	−65 20 21	434	2.9	−10.92	9.76	5

Notes. [(a)] The number in this column refers to the table where the respective line fluxes can be found.

Table 1. continued.

Name	RA(2000)[a] (h m s)	Dec(2000)[a] (d m s)	V^a_{LSR} (km s^{-1})	D^a (Mpc)	lg FIR[b] (W m^{-2})	lg L_{FIR} ($L_\odot$)	Table[a]
CGCG 049-057	15 13 13.1	+07 13 32	3897	61.9	−11.96	11.01	2
Arp 220/IC 1127	15 34 57.1	+23 30 11	5434	82.9	−11.31	11.96	2, 5
NGC 6090/Mrk496	16 11 40.7	+52 27 24	8785	126	−12.47	11.21	5
NGC 6240	16 52 58.9	+02 24 03	7339	109	−11.96	11.56	2
IRAS F17207-0014	17 23 21.9	−00 17 01	12834	183	−11.83	12.17	2
SagA*/MilkyWay	17 45 40.0	−29 00 28	0	0.0085	–	0.00	4
IC 4687	18 13 39.6	−57 43 31	5200	77.3	−12.08	11.14	2
IRAS F18293-3413	18 32 41.1	−34 11 27	5449	81.1	−11.75	11.51	2
NGC 6946	20 34 52.3	+60 09 14	385	5.5	−11.48	10.30	3, 5
NGC 7130	21 48 19.5	−34 57 04	4842	68.7	−12.06	11.06	4
NGC 7172	22 02 01.9	−31 52 11	12603	37.6	−12.45	10.08	4
NGC 7331	22 37 04.0	+34 24 56	816	14.4	−11.78	10.01	3
NGC 7469	23 03 15.6	+08 52 26	4892	67.0	−11.88	11.29	2
NGC 7469	23 03 15.6	+08 52 26	4892	67.0	−11.88	11.29	2
NGC 7552	23 16 10.7	−42 35 05	1608	22.5	−11.44	10.76	2
NGC 7582	23 18 23.5	−42 22 14	1575	22.0	−11.61	10.49	5
NGC 7771	23 51 24.8	+20 06 42	4277	58.0	−11.97	11.08	2
Mrk 331	23 51 26.8	+20 35 10	5541	74.9	−12.09	11.18	2

were taken from the IRAS point source catalog (PSC); L_{FIR} is the corresponding luminosity in solar units. This sample contains 76 galaxies, of which 22 can be classified as luminous infrared galaxies (LIRGs, $L_{FIR} \geq 10^{11}\ L_\odot$) and 6 as ultraluminous infrared galaxies (ULIRGs, $L_{FIR} \geq 10^{12}\ L_\odot$). Several of the sample galaxies contain an active galactic nucleus (AGN) in addition to the starburst that usually dominates the FIR continuum and submillimeter line emission. However, in Centaurus A, the AGN is dominating the emission over any starburst contribution.

The purpose of this paper is fourfold: (a) to present an extensive set of [C I] fluxes covering a wide range of (starbursting) galaxy centers, ranging from relatively normal galaxies to LIRGs and ULIRGs; (b) to determine the behavior of the observed [C I] lines with respect to each other, ^{12}CO, and ^{13}CO; (c) to investigate whether the derived [C I] and ^{12}CO line ratios can be used to characterize the molecular ISM of the parent galaxies without resorting to the more elaborate fitting of detailed models (PDR, XDR, CR, etc.) and at the same time to gain understanding of how the molecular gas properties define the model results; and (d) to specifically address the question of whether the [C I] line luminosity reliably traces molecular hydrogen column densities so that it can be successfully used to determine overall molecular mass.

2. DATA

2.1. Herschel-SPIRE

A large sample of (ultra)luminous galaxies was observed as part of the HerCULES program (cf. Rosenberg et al. 2015) with the Spectral and Photometric Imaging Receiver and Fourier-Transform Spectrometer (SPIRE-FTS − Griffin et al. 2010) onboard the *Herschel* Space Observatory[2] (Pilbratt et al. 2010) in the single-pointing mode with sparse image sampling. The observations are summarized in Table 2. In addition to these galaxies, we also extracted a set of more nearby galaxies from the *Herschel* Archives (mostly taken from the SINGS sample). Many of these were observed with SPIRE in spectral mapping mode, but for our purpose we only extracted the central resolution element. These data are summarized in Table 3. The FTS has two detector arrays (the SLW: wavelength range 303−671 μm corresponding to a frequency range 447−989 GHz, and the SSW: wavelength range 194−313 μm) corresponding to a frequency range 959−1544 GHz). All ^{12}CO lines in the J = 4−3 to J = 13−12 transitions were covered, as well as the two submillimeter [C I] lines. In this paper, we only discuss the [C I] lines, and the adjacent J = 4−3 and J = 7−6 ^{12}CO lines that were all observed with the SLW. The ^{12}CO (4−3) lines occurred close to the spectrum edge, and their fluxes could not be recovered in some cases, either because the noise increase at the edge made it impossible to reliably fit the line or because the line was red-shifted out of the spectrum altogether, typically at $V_{LSR} \geq 5500$ km s^{-1}. This is also the case for a smaller number of [C I] (1−0) lines in galaxies with $V_{LSR} \geq 11\,000$ km s^{-1}.

The SPIRE spectral resolution of 1.21 GHz is insufficient to resolve the lines in the SLW spectrum that contains the transitions discussed in this paper. Fluxes were first extracted using FTFitter[3], a program specifically created to extract line fluxes from SPIRE-FTS spectra. This is an interactive data language (IDL) based graphical user interface that allows the user to fit lines, choose line profiles, fix any line parameter, and extract the flux. We defined a polynomial baseline to fit the continuum, derived the flux from the baseline-subtracted spectrum and fitted it with an unresolved line profile. The beam SLW FWHM values are given in the on-line *Herschel*-SPIRE manual: 40" for ^{12}CO (4−3) and an almost identical 35" for ^{12}CO (7−6), [C I] (1−0), and [C I] (2−1). In Tables 2 and 3 we present the [C I] ^{12}CO (4−3) and ^{12}CO (7−6) line fluxes extracted from the SPIRE spectra. For a more detailed description of the data extraction and reduction method used, we refer to Rosenberg et al. (2015).

[2] *Herschel* is an ESA space observatory with science instruments provided by European-led Principal Investigator consortia and with important participation from NASA.

[3] https://www.uleth.ca/phy/naylor/index.php?page=ftfitter

Table 2. [C I] and CO line fluxes from HerCULES galaxies.

Name	Observed line flux						*Herschel*	Ref.[a]
	CO (4–3) 461 GHz	CO (7–6) 807 GHz	[C I] (1–0) 492 GHz	[C I] (2–1) 809 GHz	CO (2–1) 230 GHz	^{13}CO (2–1) 220 GHz	obsid	
	(10^{-17} W m^{-2})				(10^{-19} W m^{-2})			
NGC 34	–	2.54	0.75	1.25	10	–	1342199253	PS14
NGC 253	128	182	41.5	114	2355	229	1342210847	R14, *
MGC+12-02-001	3.07	2.69	1.05	2.59	–	–	1342213377	–
IC 1623	4.25	3.41	2.40	3.83	–	–	1342212314	–
IRAS F05189-2524	–	0.87	0.25	0.61	10	1.5	1342192833	P12, PS14
NGC 1365	41.7	26.2	19.6	31.8	385	34	1342204021	I, *
NGC 1614	2.61	3.43	1.10	2.67	95	–	1342192831	A95
NGC 2146	17.0	17.8	5.68	15.3	402	35	1342193810	I09a *
NGC 2623	1.92	2.84	0.86	2.44	21	–	1342219553	P12
NGC 3256	17.7	18.9	7.87	16.0	261	10	1342201201	S06
Arp 299C/IC 694	5.75	5.34	1.79	3.82	74	8.9	1342199250	S12, A95, *
Arp 299B	5.17	5.38	1.99	3.88	77	7.1	1342199249	S12, A95, *
Arp 299A/NGC 3690	8.71	12.0	2.44	7.81	139	6.9	1342199248	S12, A95, *
ESO 320-G030	4.39	4.54	1.72	3.44	–	–	1342210861	–
NGC 4418	1.17	5.17	1.83	1.08	–	–	1342187780	–
Mrk 231	–	2.46	0.58	1.34	24	0.45	1342210493	P12
IRAS 13120-5453	–	6.70	2.35	5.39	–	–	1342212342	–
Arp 193/IC 883	3.20	3.41	1.35	3.70	65	1.9	1342209853	P12, P14
NGC 5135	3.53	3.04	3.36	6.18	95	6.4	1342212344	P12, PS14
ESO 173-G015	12.1	17.5	4.90	14.5	–	–	1342202268	–
Mrk 273	–	2.82	0.51	1.76	21	2.6	1342209850	P12
CGCG 049-057	–	2.99	0.96	1.41	46	1.7	1342212346	P12
Arp 220	6.77	13.4	2.95	7.42	86	4.3	1342190674	P12
NGC 6240	7.78	16.6	3.04	9.54	114	1.9	1342214831	P14
IRAS F17207-0014	–	4.47	1.12	2.66	53	–	1342192829	P12
IC 4687	1.67	1.56	0.91	1.57	–	–	1342192993	–
IRAS F18293-3413	5.88	6.24	4.26	7.43	–	–	1342192830	–
NGC 7469	3.24	3.74	2.14	4.63	73	5.3	1342199252	P12, I09a, *
NGC 7552	12.4	11.6	5.46	10.8	208	22	1342198428	A95
NGC 7771	4.49	3.49	5.86	7.29	–	–	1342212317	–
Mrk 331	2.45	2.30	1.34	2.57	–	–	1342212316	–

Notes. [(a)] References to ground-based $J = 2–1$ ^{12}CO and ^{13}CO observations: A95 = Aalto et al. (1995), I09a = Israel (2009a); I = Israel (JCMT, this paper); P12 = Papadopoulos et al. (2012); P14 = Papadopoulos et al. (2014), PS14 = Pereira-Santaella et al. (2014); R14 = Rosenberg et al. (2014a); S06 = Sakamoto et al. (2006). S12 = Sliwa et al. (2012). For galaxies marked by an asterisk (*) we have determined $J = 2–1$ ^{12}CO and ^{13}CO fluxes corresponding to the SPIRE aperture by integration over the (JCMT) map.

2.2. JCMT 15 m

The 15 m *James Clerk Maxwell* Telescope (JCMT)[4] on top of Mauna Kea (Hawaii) was used between 2003 and 2005 to measure the $J = 2–1$ transitions of ^{12}CO and ^{13}CO at 230 and 220 GHz, respectively, toward a large number of galaxy centers. At the observing frequencies, the beam size was 22″ and the main-beam efficiency was 0.7. We used the facility receiver RxA3 and the Digital Autocorrelating Spectrometer (DAS). All observations were taken in beam-switching mode with a throw of 3′ in azimuth. Spectra were binned to various resolutions; we applied linear baseline corrections only and scaled the spectra to main-beam brightness temperatures. Line parameters were determined by Gaussian fitting and by adding channel intensities over the relevant range. A subset of the data has already been published (references given at the bottom of each table).

[4] The *James Clerk Maxwell* Telescope was operated by the Joint Astronomy Centre on behalf of the Science and Technology Facilities Council of the United Kingdom, the National Research Council of Canada, and (until 31 March 2013) the Netherlands Organization for Scientific Research.

2.3. Other data

In the past few years, *Herschel*-SPIRE results have been published for a variety of galaxies. Both [C I] line fluxes and those of the ^{12}CO (4–3) and ^{12}CO (7–6) lines in these galaxies are given in Table 4. The [C I] (1–0) 492 GHz and adjacent ^{12}CO (4–3) 461 GHz line fluxes of galaxies measured from the ground are given in Table 5. In Tables 2, 4, and 5 we have also included $J = 2–1$ ^{12}CO and ^{13}CO line fluxes, when available. For the distant high-luminosity sources, most of these derive from JCMT or IRAM 30 m observations. In general, these objects have (CO) sizes that are smaller than the observing beam (see Papadopoulos et al. 2012). For the nearer and more extended galaxies, we used JCMT or SEST observations with a beam size of 22”. Exceptions are the observations of Arp 299 taken from Aalto et al. (1995: NRAO 12 m, 28″) and Sliwa et al. (2012: integrated over a combined SMA/JCMT map covering the source – see Rosenberg et al. 2014b). The data on M 82 were taken from Ward et al. (2006) and cover the inner lobes. The data on NGC 4945 and the Circinus galaxy were taken from Hitschfeld et al. (2008: *Nanten2*, 38″) and Zhang et al. (2014; APEX, 14″,

Table 3. [C I] and CO line fluxes from *Herschel* archive galaxies.

Name	Observed line flux						*Herschel*	Ref.[a]
	CO (4–3) 461 GHz	CO (7–6) 807 GHz	[C I] (1–0) 492 GHz	[C I] (2–1) 809 GHz	CO (2–1) 230 GHz	^{13}CO (2–1) 220 GHz	obsid	
	(10^{-17} W m^{-2})				(10^{-19} W m^{-2})			
NGC 1275/Per A	0.86	0.56	0.48	1.05	13	2.0	1342249055	BI98
NGC 1482	0.52	0.19	0.32	0.61	61	–	1342248233	A07
NGC 2798	1.48	2.65	0.67	2.11	–	–	1342252892	
NGC 3521	0.49	0.09	0.59	0.50	–	–	1342247743	
NGC 3627/M66	0.80	0.26	0.68	0.61	92	7.3	1342247604	I
NGC 4254/M99	0.82	0.18	1.14	1.20	58	5.4	1342236997	I
NGC 4321/M100	0.60	0.18	0.38	0.47	100	7.8	1342247572	I
NGC 4536	1.71	1.99	0.23	2.27	90	7.4	1342237025	I
NGC 4631	1.65	0.57	0.83	1.60	119	5.5	1342247553	I09a, *
NGC 4736/M94	0.68	0.26	0.51	0.86	69	5.9	1342245851	GP00, Ba06
NGC 4826/M64	0.75	0.34	0.82	1.04	301	40	1342246992	IB02, I09a, *
NGC 4945	34.9	90.8	21.5	91.7	1570	131	1342212343	W04
NGC 5055/M63	1.08	0.31	0.95	1.60	78	13	1342237026	I
NGC 5194/M51	1.67	0.62	1.21	2.36	205	28	1342201202	IB02, ITB, *
NGC 5713	0.57	0.23	0.26	0.42	49	5.6	1342248250	I
Circinus	41.3	36.2	17.1	41.8	592	56	1342251313	H08
NGC 6946	5.07	5.74	2.20	5.36	789	79	1342243603	IB01, IB02, *
NGC 7331	1.03	0.16	0.56	0.95	20	3.4	1342245871	IB99, *

Notes. [(a)] References to ground-based $J = 2–1$ ^{12}CO and ^{13}CO observations: A07 = Albrecht et al. (2007); Ba06 = Bayet et al. (2006); BI98 = Bridges & Irwin (1998); GP00 = Gerin & Phillips (2000); H08 = Hitschfeld et al. (2008); I09a = Israel (2009a); I = Israel (JCMT, this paper); IB01 = Israel & Baas (2001); IB02 = Israel & Baas (2002); ITB = Israel et al. (2006); W04 = Wang et al. (2004). For galaxies marked by an asterisk (*) we have determined $J = 2–1$ ^{12}CO and ^{13}CO fluxes corresponding to the SPIRE aperture by integration over the (JCMT) map.

Table 4. Published *Herschel*-SPIRE [C I] and CO line fluxes.

Name	Observed line flux						Ref.[a]
	CO (4–3) 461 GHz	CO (7–6) 807 GHz	[C I] (1–0) 492 GHz	[C I] (2–1) 809 GHz	CO(2–1) 230 GHz	^{13}CO (2–1) 220 GHz	
	(10^{-17} W m^{-2})				(10^{-19} W m^{-2})		
NGC 1056	–	0.61	–	0.77	10.4	–	PS13
NGC 1068/M 77	21.7	21.1	12.8	21.1	866	76	Sp12, P12*
IRAS 09022-3615	–	3.33	1.22	1.52	–	–	
UGC 05101	–	1.05	–	1.28	9.7	0.13	PS13
NGC 3034/M 82	113	209	33.8	117	2070	142	P10, W03*
NGC 3227	2.90	1.81	2.27	4.66	26.5	6.9	PS13, I
NGC 3982	1.81	0.47	–	1.00	4.3	–	PS13
NGC 4038	5.47	1.48	1.00	1.86	88.2	3.7	Sc14, I
NGC 4039	2.92	1.85	1.65	2.41	109.6	7.7	Sc14, I
NGC 4051	–	0.73	–	0.78	24.9	1.3	PS13, I
NGC 4151	–	0.36	–	0.84	3.0	–	PS13
NGC 4388	2.39	1.31	1.45	2.67	5.5	–	PS13
IC 3639	1.21	–	–	0.58	20.9	–	PS13
NGC 5128/Cen A	11.3	4.16	11.5	30.2	172	12	I14*
NGC 5236/M 83	11.5	8.82	4.54	14.0	582	62	K14, IB01, *
NGC 7130	3.30	2.55	1.64	2.67	44.9	–	PS13
NGC 7172	–	–	3.82	4.50	26.0	–	PS13
NGC 7582	6.93	6.56	3.44	7.59	139	–	PS13, A95
MilkyWay ($\times 10^{-6}$)	2.70	1.52	1.68	1.68	0.98	—	F99

Notes. [(a)] Reference to line fluxes: A95 = Aalto et al. (1995), F99 = Fixsen et al. (1999) – COBE measurement; I14 = Israel et al. (2014); I = Israel (JCMT, this paper); K14 = Kamenetzky et al. (2014) P10 = Panuzzo et al. (2010); P12 = Papadopoulos et al. (2012), P14 = Papadopoulos et al. (2014); PS13 = Pereira-Santaella et al. (2013); PS14 = Pereira-Santaella et al. (2014); Sc14 = Schirm et al. (2014); Sp12 = Spinoglio et al. (2012); W03 = Ward et al. (2003). For galaxies marked by an asterisk (*) we have determined $J = 2–1$ ^{12}CO and ^{13}CO fluxes corresponding to the SPIRE aperture by map integration.

Table 5. Published ground-based [C I] and CO line fluxes.

Name	Observed line flux[a]						Ref.[b]
	CO (4−3) 461 GHz	CO (7−6) 807 GHz	[C I] (1−0) 492 GHz	[C I] (2−1) 809 GHz	CO (2−1) 230 GHz	^{13}CO (2−1) 220 GHz	
	(10^{-17} W m^{-2})				(10^{-19} W m^{-2})		
IC10	0.89	1.00	0.52	0.84	25	1.4	GP00, Ba06
NGC 253	101	–	31.5	–	1210	104	IWB, IB02
NGC 278	0.89	–	0.54	–	17.9	1.9	IB02, I09b
NGC 660	8.39	–	3.37	–	154	11	IB02, I09b
NGC 891	–	–	0.79	–	118	12	Ba06, I
Maffei 2	40.6	–	2.17	–	275	22	IB02, IB03
NGC 1068	10.8	–	5.33	–	247	17	IB02, I09a
IC 342	20.6	–	2.94	–	193	24	IB02, IB03
Henize2-10	1.40	4.00	0.36	–	20	1.2	GP00, Ba06
NGC 3079	11.4	–	7.61	–	189	11	IB02, I09b, GP00
NGC 3628	10.9	–	4.13	–	169	13	IB02, I09b
NGC 4038	2.6	0.6	0.94	–	110	14	GP00, Ba06
NGC 4736/M94	–	–	0.57	–	69	5.9	GP00, Ba06
NGC 4826/M64	8.49	–	5.11	–	126	15	IB02, I09a
NGC 4945	56.8	–	80.4	–	1300	131	H08
NGC 5194/M51	2.76	–	1.41	–	43.5	5.7	IB02, ITB, GP00
NGC 5236/M83	26.7	–	5.98	–	291	28	IB01, IB02
Circinus	18.0	26.1	8.20	–	592	56	H08, Z14
NGC 6090/Mrk496	–	–	0.38	–	43	–	GP00, Ba06
NGC 6946	21.3	–	4.78	–	249	22	IB01, IB02, GP00

Notes. In this table only, all fluxes refer to the same beamwidth of 22", except in the cases of NGC 4945 and the Circinus galaxy where beamwidths of 38" apply, similar to the SPIRE aperture.[(b)] Reference to line fluxes: Ba06 = Bayet et al. (2006); GP00 = Gerin & Phillips (2000); H08 = Hitschfeld et al. (2008); IWB = Israel et al. (1995); ITB = Israel et al. (2006); IB01 = Israel & Baas (2001); IB02 = Israel & Baas (2002); IB03 = Israel & Baas (2003); I09a = Israel (2009a); I09b = Israel (2009b); Z14 = Zhang et al. (2014).

corrected to 22″). For the nearby extended galaxies, the [C I] and ^{12}CO fluxes closely represent the emission from the bright central concentrations of gas and dust quite well, but not at all the more extended disk emission. In contrast, in the much more distant luminous galaxies, the emission samples all of the galaxy. Finally we note that several galaxies, especially the brighter ones, such as NGC 253, NGC 1068, and the Circinus galaxy, are found in both the SPIRE sample and the ground-based sample.

2.4. Errors

Most of the data presented in this paper were obtained with the SPIRE instrument. The error budget is discussed in some detail by Rosenberg et al. (2015). The absolute flux values in Tables 2–4 have an absolute calibration uncertainty of 6%. To this must be added another systematic uncertainty of 10% associated with baseline definition and flux extraction. Sources unresolved by the SPIRE instrument thus have an absolute flux uncertainty $\Delta F = 15\%$. In the case of resolved sources, the correction procedure used adds another 15% to this: $\Delta F = 30\%$. Since systematic errors dominate, the line ratios are much more accurate, notably the ratios between the lines that are close in frequency, i.e., the [C I](1−0) and CO(4−3) lines and the [C I](2−1) and CO(7−6) line. Although hard to quantify, their uncertainty should be on the order of five per cent or less in almost all cases listed.

The ground-based JCMT $J = 2{-}1$ ^{12}CO and ^{13}CO line fluxes have typical uncertainties of $\Delta F = 20\%$ associated with antenna, receiver, and atmospheric calibration. Thus, the ^{12}CO/^{13}CO line ratios that refer to very similar beams have an uncertainty of about 30%. The ratios of SPIRE CO(4−3) and [C I](1−0) to JCMT $J = 2{-}1$ ^{12}CO and ^{13}CO have uncertainties ranging from 25% for compact sources to 35% for extended objects. In a number of cases, a mismatch in beamsize may introduce an additional systematic error. This is further discussed in Sect. 3.1.

3. Results

3.1. Sample properties and line ratios

For the sample presented in this paper, we attempted to identify all galaxies that have good signal-to-noise measurements of at least one [C I] line and two supporting ^{12}CO or ^{13}CO lines. The final selection includes 76 galaxies with distances ranging from the Local Group to 250 Mpc, with nine galaxies having distances of more than 100 Mpc. The set of line fluxes is not complete, however. There are [C I] (1−0) and (2−1) line fluxes for 64 galaxies each. The sample for the ^{12}CO (2−1), (4−3), and (7−6) lines consists of 61, 58, and 62 galaxies, respectively. Finally, ^{13}CO (2−1) fluxes are available for 46 galaxies. The set of ^{12}CO and [C I] line fluxes is complete for a total of 35 galaxies, and we will refer to these galaxies as the complete subsample. In our subsequent analysis, we give preference to the SPIRE data whenever a galaxy was observed both from the ground and from space.

Because the SPIRE measurements were obtained with very similar beam sizes, we can construct [C I] (2−1)/(1−0), ^{12}CO (7−6)/(4−3), ^{12}CO (4−3)/[C I] (1−0), and ^{12}CO (7−6)/[C I] (2−1) ratios that can be directly compared to one another. The ground-based measures of the $J = 2{-}1$ ^{12}CO and ^{13}CO emission are likewise determined in almost identical beams, but these are generally smaller than the SPIRE beam. This complicates the comparison of line ratios containing either of these two transitions: the difference in beam sizes may cause a flux bias where

Table 6. Average line ratios.

Ratio	Complete subsample		Total sample		(U)LIRG	Starburst
	n	average	n	average	Subsample	
[C I](2−1)/[[C I](1−0)	35	2.08 ± 0.11	63	2.12 ± 0.11	2.17 ± 0.13	1.86 ± 0.12
CO(4−3)/CO(2−1)	35	4.22 ± 0.41	55	5.08 ± 0.42	5.80 ± 0.73	4.27 ± 0.39
CO(7−6)/CO(4−3)	35	0.84 ± 0.09	57	0.97 ± 0.10	1.11 ± 0.10	0.90 ± 0.15
[C I](1−0)/CO(4−3)	35	0.48 ± 0.04	62	0.46 ± 0.03	0.47 ± 0.04	0.46 ± 0.03
[C I](2−1)/CO(7−6)	35	2.03 ± 0.30	66	1.67 ± 0.19	0.92 ± 0.08	2.19 ± 0.29
[C I](1−0)/^{13}CO(2−1)	35	32.6 ± 5.5	49	33.2 ± 4.5	59.1 ± 12.3	23.9 ± 2.1
CO(sum)/[C I](sum)	35	1.25 ± 0.09	60	1.25 ± 0.06	1.39 ± 0.10	1.16 ± 0.09

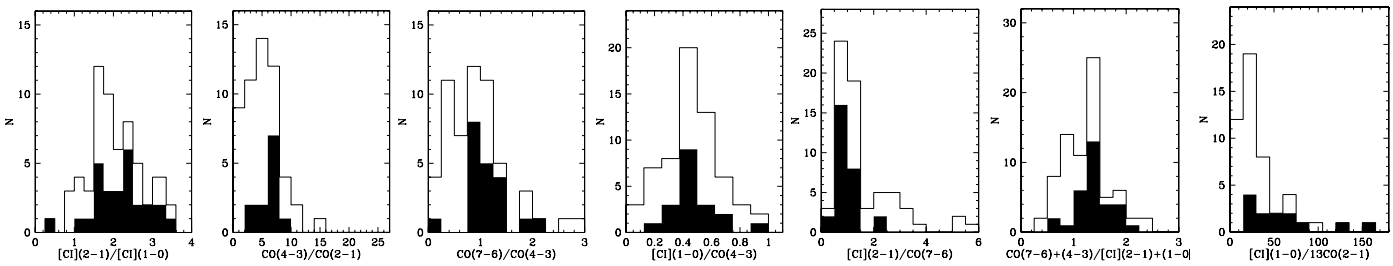

Fig. 1. Distribution of the various [C I] and CO line flux ratios over the total sample of galaxies. The subsample of luminous galaxies (LIRGS and ULIRGS) is indicated by the shaded area.

the ground-based emission is underestimated by a factor of about three. However, in a number of cases, the $J = 2-1$ ^{12}CO emission was mapped, which allowed us to convolve the ground-based data to the SPIRE resolution. In the tables, these cases are indicated by an asterisk in the last column. A comparison of the full resolution and the convolved ^{12}CO (2−1) fluxes shows that the correction varies from galaxy to galaxy, but is usually less than a factor of two (see also Kamenetzky et al. 2014; and Ueda et al. 2014).

In Fig. 1 we show the distribution of the various line ratios derived from the sample, and Table 6 summarizes the averages. Because not all galaxies are measured in all lines, the question arises whether or not a further bias is introduced by comparing line ratios derived from different subsamples. As is clear from Table 6, the line ratios of the total (inhomogeneous) sample and those of the complete subsample are within the errors identical with the marginal exception of the ^{12}CO(4−3)/(2−1) ratio.

The ^{12}CO (7−6)/(4−3) flux ratio ranges from 0.3 (low excitation) to 3 (high excitation), with a peak at a ratio of unity. (If we had expressed the CO line ratio not in flux but in brightness temperature $T_{\rm mb}$, we would have found the peak to be at a ratio $T_{\rm mb}(7-6)/T_{\rm mb}(4-3) = 0.2$.) The distributions of the other line ratios are more clearly peaked, suggesting that the measured lines stem from physical conditions that do not vary greatly over the sample galaxies. We note that the [C I] (1−0) line is usually weaker by a factor of about two than the adjacent ^{12}CO (4−3) line. The [C I] (2−1)/(1−0) ratio is more broadly distributed between values of 1 and 3. The starburst galaxies have a ratio peaking at 1.9, and the more luminous (U)LIRGs peak at about 2.2. This is very close to the mean [C I] (2−1)/(1−0) ratio of 2.4 ± 0.3 measured by Walter et al. (2011) for nine galaxies at redshifts $z = 2.2-6.4$. In the high-density, low-temperature case, a ratio of two corresponds to a kinetic temperature $T_{\rm kin} = 25$ K; conversely, in the low-density, high-temperature case the parent gas should have a density of $n \approx 135$ cm^{-3}.

The ratio of the [C I] (1−0) and ^{13}CO fluxes is of interest because both lines are expected to be optically thin, in contrast to the ^{12}CO lines that are optically thick. The rightmost panel in Fig. 1 shows a distribution with a peak at 25 and a long tail stretching out to NGC 6240, with a ratio of 158. The major peak already corresponds to a brightness-temperature ratio over 2, which is much higher than the typical values of 0.3−0.5 found in Milky Way star-forming complexes (cf. IB02).

In Fig. 1, we show both the total sample and the luminous-galaxy ($L \geq 10^{11}$ $M_\odot$) subsample. Statistically, the separation is not "clean", because the low-luminosity galaxies tend to be at much closer distances. If they experience an intense but relatively small-scale circumnuclear starburst, our ratios may nevertheless locally sample the same physical conditions that occur in LIRGs globally. As Table 6 also shows, the LIRGs have clearly higher CO(7−6)/[C I](2−1) and [C I]/ ^{13}CO ratios. In their [C I](2−1)/(1−0), CO(7−6)/(4−3), CO(4−3)/CO(2−1), and CO(4−3)/[C I](1−0) ratios, the LIRGs and less luminous starburst galaxies do not differ much, although the LIRGS tend to have marginally higher ratios.

Almost all of the fifty galaxies detected in both $J = 2-1$ CO isotopes have an isotopic ratio below 20, with a mean of about 12. Six galaxies have elevated ratios between 20 and 40, and three galaxies (the mergers NGC 3256, Mrk 231, NGC 6240) have very high isotopic ratios between 50 and 70. We note, however, that galaxies with low isotopic ratios are much easier to detect in ^{13}CO emission. Thus, the statistics are biased against very high isotopic ratios.

3.2. Relation between [C$_{\rm I}$] and ^{12}CO

In Fig. 2a we compare the [C I]-to-adjacent-CO line ratios for all detected galaxies. As we have already seen in Fig. 1, the CO(4−3) line is stronger than the [CI] (1−0) line with very few exceptions. Only Centaurus A, NGC 5135, NGC 3521, NGC 4254, and NGC 4826 have stronger [C I] (1−0) lines. The situation for NGC 4945 and the Circinus galaxy is unclear. The *Nanten2* measurements by Hitschfeld et al. (2008) clearly show the [C I] line to be the stronger (Table 5, but both the *Herschel*-SPIRE, and the APEX measurements clearly show the ^{12}CO (4−3) line to be the strongest. The difference in beam

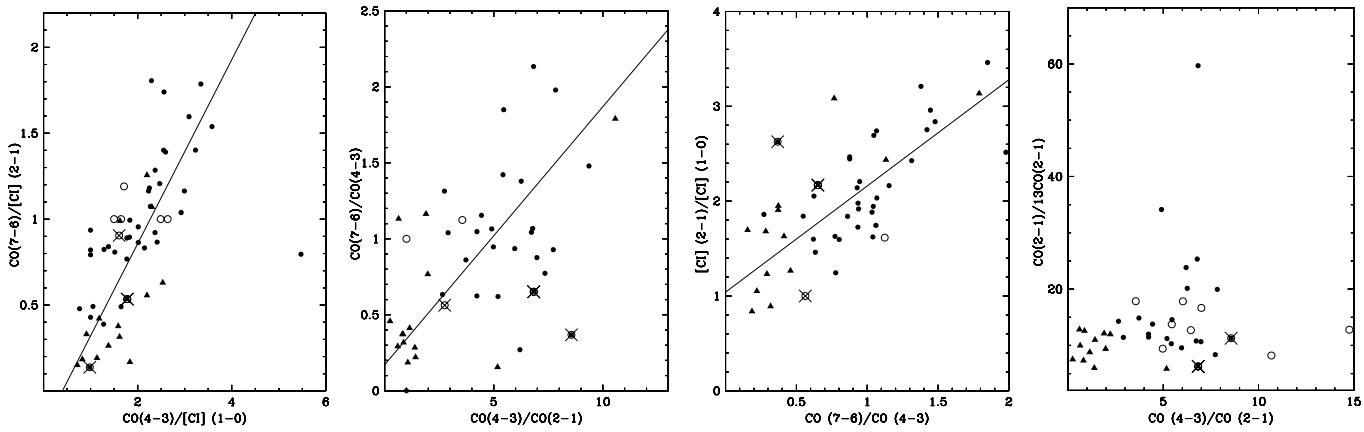

Fig. 2. Line flux ratio diagrams for the sample galaxies. Ratios derived from *Herschel*-SPIRE data are marked by filled circles (single pointings) and filled triangles (map central peak), those derived from ground-based observations are denoted by open circles. Points corresponding to Centaurus A, Perseus A, and the Milky Way are indicated by an additional cross. a. (*left*) [C I] lines compared with adjacent CO lines. The linear regression correlation marked in the panel has a slope of 0.55, and a correlation coefficient $r^2 = 0.66$. b. (*second from left*) CO transition line ratios are likewise correlated with a slope of 0.17 and $r^2 = 0.37$. c. (*second from right*) [C I] line ratio versus the ratio of their neigbouring CO lines, slope 1.12 and $r^2 = 0.67$. d. (*right*) $J = 2{-}1$ CO isotopic ratio as a function of the CO (4−3)/CO (2−1) ratio; no obvious correlation although the dispersion increases with CO ratio.

sizes cannot explain this contradictory result. A similar discrepancy occurs for NGC 4826, where the ground-based observations show the [C I] (1−0) line to be weaker than the ^{12}CO (4−3) line. In this case, however, the difference in observing beam size (22" versus 38") may be relevant.

As far as the ^{12}CO (7−6)/[C I](1−0) line ratio is concerned, Centaurus A has the lowest ratio in the whole sample, although ratios that are almost as low are also found for NGC 3521, NGC 4254, NGC 5055, and NGC 7331. The exceptional nature of Centaurus A has already been noted by Israel et al. (2014), who drew attention to the high flux of both [C I] lines with respect to the spectrally adjacent ^{12}CO lines. The Centaurus A center is almost unique in having both a [C I] (1−0) 492 GHz line flux exceeding that of the ^{12}CO (4−3) 461 GHz line and a [C I] (2−1) 809 GHz line that is more than seven times stronger than the ^{12}CO (7−6) 806 GHz line. In contrast, the CO-to-C ratios of the other radio galaxy, Perseus A, do not stand out in any way. As Fig. 2a also shows, the CO(4−3)/[C I](1−0) and CO(7−6)/]*ci*(2−1) line ratios are well correlated, with NGC 4536 as an outlier.

There are relatively good correlations between the CO(7−6)/CO(4−3) and the CO(4−3)/CO(2−1) ratios (Fig. 2b) and between the [C I] (2−1)/(1−0) and the CO(7−6)/(4−3) ratios (Fig. 2c). As these figures suggest, there is also a reasonable correlation between the [C I] (2−1)/(1−0) and the CO(4−3)/CO(2−1) ratios, although this suffers from larger scatter than the relation shown in Fig. 2c. Because the CO transition ratios provide a rough indication of the degree of excitation of the molecular gas, it thus follows that higher [C I] ratios go with more highly excited gas. The models by Meijerink & Spaans (2005), Meijerink et al. (2007), and Kazandjian et al. (2012) show that the higher ^{12}CO ratios in Figs. 2b and 2c are inconsistent with heating by UV photons (PDRs) alone and should be associated with either X-rays or mechanical heating from turbulence and shocks. Although the correlation between the [C I] line ratios and the ^{12}CO line ratios is quite evident in Fig. 2c, it has a significant dispersion. By itself, the Centaurus A [C I] (2−1)/(1−0) ratio is not exceptional, but it is relatively high for its location in the diagram, which corresponds to a low degree of excitation as indicated by the ^{12}CO (7−6)/(4−3) ratio.

Finally, the $J = 2{-}1$ ^{13}CO/^{12}CO isotopic ratios do not appear to be clearly correlated with the ^{12}CO (4−3)/(2−1) (or either the [C I] (2−1)/(1−0) line ratio or the FIR luminosity for that matter). In Fig. 2d, over forty galaxies have $J = 2{-}1$ isotopic ratios below 20. The isotopic ratio does not noticeably change with increasing ^{12}CO (4−3)/(2−1) ratio. Six galaxies (Arp 193, Arp 220, Arp 299A, NGC 3256, NGC 4038, and CGCG 049-057) have ratios between 20 and 40, and only Markarian 231, UGC 05101, and NGC 6240 have very high isotopic ratios between 50 and 70, signifying both low CO optical depths and high intrinsic ^{12}C/^{13}C abundance ratios (see also Martín et al. 2010; Henkel et al. 2014). However, there does not appear to be a preferred range in [C I] or CO line ratios for the highest isotopic ratios.

3.3. Relation between [C$_I$] and ^{13}CO

A direct comparison of [C I] and ^{13}CO line intensities is of interest because both are thought to be optically thin (in contrast to the ^{12}CO transitions measured, which are optically thick). These comparisons were made for small samples of galaxies by Gerin & Phillips (2000) and by Israel & Baas (2002; hereafter IB02). A major and unexpected result of the latter study was the discovery that in galaxy centers the [C I] (1−0)/^{13}CO (2−1) ratio increases with the (carbon) line luminosity. In the IB02 sample, most galaxy centers exhibited a [C I]/^{13}CO brightness temperature ratio exceeding the value 0.3−0.5 that is the rule for (UV) PDRs in the Milky Way galaxy. This finding was supported by observations of NGC 4945 and the Circinus galaxy Hitschfeld et al. (2008). The present, much larger sample expanded by both the new (Tables 2, 3) and published (Table 4) SPIRE results confirm the positive correlation (ratio increasing with luminosity) found by IB02. In Fig. 3a we show the [C I] (1−0)/^{13}CO (2−1) ratio as a function of the [C I] (1−0) luminosity. This figure corresponds to the left-hand panel of Fig. 2 in IB02, with the difference that we now use metric flux ratios and luminosities instead of values based on brightness temperatures. The new data extend the previously found correlation up to ULIRGs, so that it now covers over three decades in luminosity. The correlation is robust because it remains present

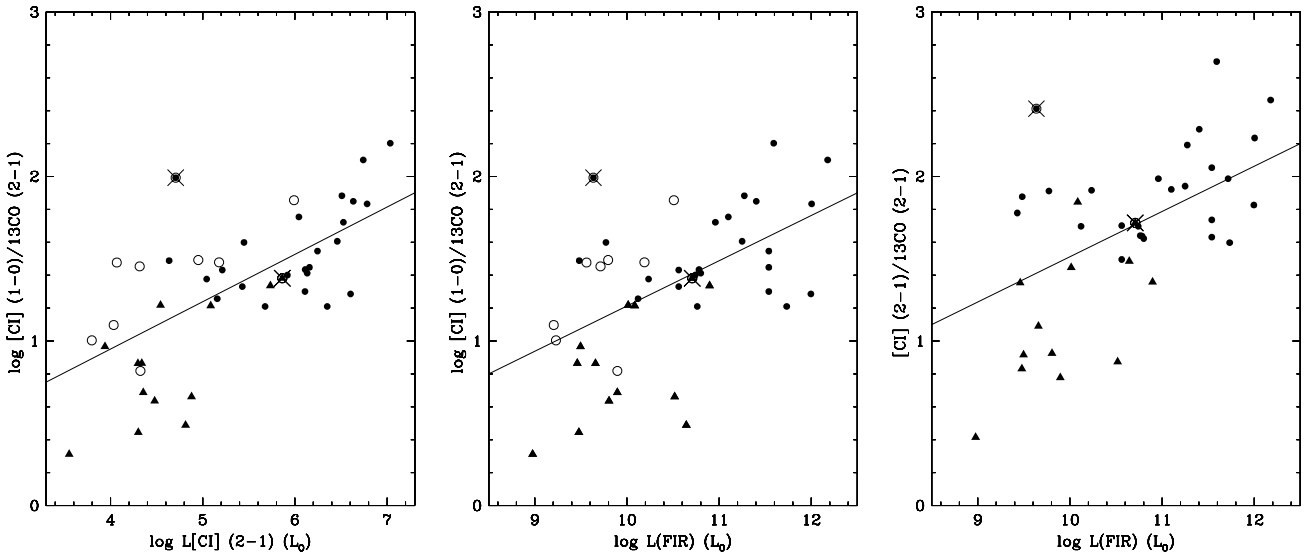

Fig. 3. Flux ratio of the [C I] $J = 1{-}0$ to ^{13}CO $J = 2{-}1$ line in the sample galaxies as a function of the [C I] $J = 1{-}0$ luminosity (*left*), and the total FIR luminosity (*center*); the panel on the right depicts the ratio of the [C I] $J = (2{-}1)$ line to the ^{13}CO line, again as a function of FIR luminosity. As in the previous figure, ratios derived from *Herschel*-SPIRE data are indicated by filled circles and filled squares, those derived from ground-based observations by open circles. Centaurus A and Perseus A are indicated by an additional cross. Linear regression correlation slopes and coefficients are *from left to right*: 0.27/0.42, 0.26/0.28, 0.28/0.32.

whether the [C I] $(1{-}0)/^{13}$CO $(2{-}1)$ ratio is plotted as a function of the [C I] line, the ^{13}CO $(2{-}1)$ line, or even the IRAS-derived FIR continuum luminosity. The emission of the sample galaxies is mostly due to starbursts, dominating any AGN that may be present. Notable exceptions are Centaurus A (NGC 5128) and Perseus A (NGC 1275), which are dominated by an AGN rather than a starburst. Perseus A has "normal" ratios, but Centaurus A is an outlier with relatively strong [C I] emission for its modest FIR luminosity. The significant increase in [C I] $(1{-}0)$ line fluxes with increasing luminosity is thus well-established and shared by the [C I] $(2{-}1)$ line (Fig. 3c). Both $J = 1{-}0$ and the $J = 2{-}1$ [C I] to ^{13}CO $(2{-}1)$ line ratios increase with (FIR) luminosity.

4. Line ratios and LVG models

4.1. Diagnostic panels

To extract physical information from the gas in which the line emission originates, we evaluated the observed line ratios using the large-velocity gradient (LVG) radiative transfer code RADEX described by Jansen (1995), Jansen et al. (1994), and Hogerheijde & van der Tak (2000)[5]. LVG models have the advantage of not requiring any prior specification of a particular chemical or heating model. The LVG code provides model line intensities as a function of three input parameters: gas kinetic temperature (T_k), molecular hydrogen density ($n(H_2)$), and the CO (or C) gradient, i.e. the column density per unit velocity (N(CO)/dV resp. N(C)/dV). In our analysis, we explored, the parameter range $T_k = 10{-}200$ K, $n(H_2) = 10^2{-}10^8$ cm^{-3}, $N(^{12}\mathrm{CO})/\mathrm{d}V = (0.1{-}300){\times}10^{17}$ cm^{-2}/ km s^{-1}, $N(^{13}\mathrm{CO})/\mathrm{d}V = (0.1{-}300) \times 10^{15}$ cm^{-2}/ km s^{-1}, and N(C)/dV $= (0.1{-}30) \times 10^{17}$ cm^{-2}/ km s^{-1}. We use the diagnostic diagrams to constrain the kinetic temperature and gas density, as well as the C°/ ^{12}CO and the C°/ ^{13}CO abundance.

We do not attempt to fit all the sample galaxies individually. Rather, we consider a narrow range of cases in order to identify representative physical parameters and trends. This is possible because, as noted, the ^{12}CO $(7{-}6)/(4{-}3)$ and the ^{12}CO $(4{-}3)/(2{-}1)$ ratios of the sample galaxies increase more or less linearly with the [C I] $(2{-}1)/$[C I] $(1{-}0)$ ratio, and the ^{12}CO $(7{-}6)/$[C I] $(2{-}1)$ increases linearly with the ^{12}CO $(4{-}3)/$[C I] $(1{-}0)$ ratio. Figure 2, which illustrates this, also shows that regardless of the form and degree of correlation, most of the observed line ratios discussed in this paper cover only a limited range (see also Fig. 1).

The complete analysis only involves galaxies for which all six lines have been measured (three ^{12}CO lines, two [C I] lines, and one ^{13}CO line). Because almost all galaxies observed from the ground lack measurements of the high-frequency [C I] $(2{-}1)$ and ^{12}CO $(7{-}6)$ lines, the analysis is almost exclusively based on the *Herschel*-SPIRE sample. About half of this sample refers to very luminous galaxies, mostly LIRGs. ULIRGS tend to be at greater distances, with the consequence that the $J = 4{-}3$ ^{12}CO line and often also the [C I] $(1{-}0)$ line are red-shifted out of the SPIRE band, or suffer from excessive noise at the band edge. There is only one ULIRG (Arp 220) for which all six necessary line fluxes are available.

4.2. [C$_I$] line ratios: setting the scene

The full range of observed [C I] $(2{-}1)/(1{-}0)$ ratios is rather limited, and almost fully contained between the values of 1.5 and 3. In Fig. 4 we show the result for the modeled [C I] $(2{-}1)/(1{-}0)$ ratio at discrete values of 1, 2, and 3 over the full range of densities and temperatures defined above, as a function of three values for N(CI)/dV column densities covering an order of magnitude. In Fig. 4, the line ratios exhibit a characteristic double degeneracy for temperature and density. For any given line ratio, the emitting gas is not uniquely located in the diagram, but may be at a relatively well-determined low density with an unconstrained temperature (vertical branch), or at an unconstrained but relatively high density with a well-determined temperature. The emitting gas may even be a mixture of such phases which are indistinguishable observationally.

[5] See also http://www.strw.leidenuniv.nl/home/michiel/ratran/

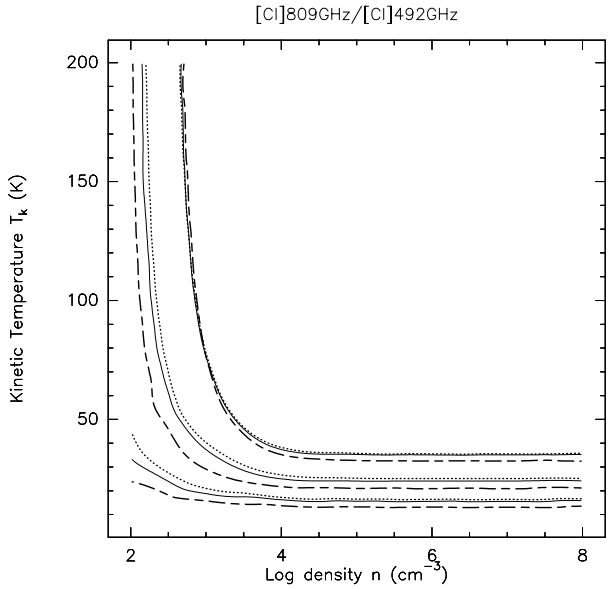

Fig. 4. LVG results for the [C I] line flux ratios observed in the galaxy sample. The panel contains lines of constant model flux ratio, as a function of H_2 gas kinetic temperature T_k and volume density $n(H_2)$, for distinct C column densities N_C/dV. Curves are depicted in groups of constant line ratio [C I](1−0)/[C I](2−1) = 1 (left, bottom), 2 (middle), and 3 (right, top). Within each group of ratios, curves are drawn for column densities $N(C)/dV = 0.3 \times 10^{17}$ cm^{-2}/ km s^{-1} (dotted line), 1×10^{17} cm^{-2}/ km s^{-1} (continuous solid line), and 3×10^{17} cm^{-2}/ km s^{-1} (dashed line), respectively.

In the diagrams, higher line ratios are found above lower line ratios i.e. a higher observed line ratio implies a shift to the right (higher densities) and to the top (higher temperatures). For any given line ratio, the curve in the diagram also shifts up and the right when the column density (abundance) is lowered, down and to the left when the abundance is increased. As Fig. 4 shows, increasing the carbon column density from the reference value $N(C)/dV = 10^{17}$ cm^{-2} km s^{-1} does not shift curves of constant line ratio by much, and lowering the carbon column density has even less effect. This reflects the fact that throughout most of the diagram in Fig. 4 the carbon lines are optically thin; optical depths exceeding unity only occur in the lower left corner of the panel.

At the highest observed [C I] (2−1)/(1−0) ratios of three, gas at temperatures above $T_k = 40$ K requires densities to be limited to $n \leq 1000$ cm^{-3}; for ratios of unity, high temperatures are only allowed at very low densities ($n \leq 100$ cm^{-3}). Galaxies that exhibit this ratio most likely instead contain gas at a well-defined temperature of 15 K, but with an undetermined density. It is evident from Fig. 4 that the observed [C I] line ratios do constrain the underlying physical conditions, and in particular rule out the presence of significant contributions to the neutral carbon emission by gas that is both dense and warm. However, beyond this, not much more can be concluded from the [C I] emission line ratio. Further progress requires breaking the T_k/n degeneracy by comparing emission from [C I] to that of other species, such as ^{12}CO.

4.3. [C I] and ^{12}CO line ratios: temperature and density

The two CO line ratios considered in this paper likewise fall within well-defined, relatively narrow ranges. All observed ^{12}CO (7−6)/(4−3) ratios fall in the range 0.25−2.0, and the ^{12}CO (4−3)/(2−1) ratios are all in the range 2 to 10. The scatter in the latter ratio to some extent reflects that not all ^{12}CO (2−1) refer to the beam defined by the SPIRE aperture in which the ^{12}CO (4−3) fluxes were measured. Although in those galaxies the difference in beam size may be as much as a factor of three, we have verified that in actual cases, the flux difference is less than a factor of two because the CO is centrally concentrated. In Fig. 5 we show T_k, n diagrams with modeled ^{12}CO (7−6)/ ^{12}CO (4−3), ^{12}CO (4−3)/ ^{12}CO (2−1), and [C I] (2−1)/[C I] (1−0) line ratios.

As we have noted before, Fig. 2 shows that the [C I] and ^{12}CO line ratios are correlated. We have determined the best-fit parameters for [C I] (2−1)/[C I] (1−0) ratios of 1.5, 2, and 2.5 and the correspondingly increasing ^{12}CO (4−3)/ ^{12}CO (2−1) and ^{12}CO (7−6)/ ^{12}CO (4−3) ratios for a range of CO abundances (N_{CO}/dV). The three diagrams in Fig. 5 show curves for [C I] (2−1)/(1−0) = 1.5, 2.0, and 2.5 and the mean CO ratios corresponding to each of these values. Each of the two CO ratios is represented by three curves for different CO abundances (N_{CO}/dV). As in Fig. 4, the CO curves in Fig. 5 exhibit the well-known double degeneracy for temperature and density. However, each of the three sets of degenerate curves is offset from the others.

If we assume that the three ^{12}CO lines (J = 2−1, J = 4−3, J = 7−6) and the two [C I] (J = 1−0, J = 2−1) lines originate in the same gas phase dominated by a single temperature and a single density, these can be found from the overlap or intersection of the relevant curves corresponding to the observed line ratio. This determination is independent of the actual [C I]/ ^{12}CO abundance (which we determine later, see Sect. 4.4). From Fig. 5 it is clear that common intersections providing solutions for T_k and n all occur at low temperatures in the range of 20−40 K, and intermediate densities in the range of 10^4−10^5 cm^{-3}. The assumption that the ^{12}CO and [C I] emitting volumes refer to the same gas cloud population is supported by the coincidence of the CO/CO and [CI]/CO intersections.

Emission characterized by ratios [C I] (2−1)/(1−0) ≤ 1.5 – i.e., with [C I] (1−0) emission relatively strong with respect to both [C I] (2−1) and ^{12}CO (4−3) – are hard to fit at all. Emission from the center of the radio galaxy Centaurus A falls into this category. For C° column densities equal to or higher than CO column densities, i.e. abundances [C]/[CO] ≥ 1.0, marginal fits to the observed CO line ratios occur only at ratios [C I] (2−1)/(1−0) ≥ 2, at modest kinetic temperatures of 25−30 K but very high densities in excess of 10^6 cm^{-3}. The quality of the fits improves with increasing CO column density, i.e. decreasing [C]/[CO] abundance. As all fits occur in the medium-density, low-temperature regime, the [C I] line ratios can be translated more or less directly into kinetic temperatures, with T_k smoothly increasing from 20 to 35 K as [C I] (2−1)/(1−0) increases from 1.5 to 3.0. The fitted density depends weakly on the column densities assumed. For instance, at constant T_k = 30 K and abundance [C]/[CO]=0.3, we find log n = 5.5 ± 0.5, log n = 4.6 ± 0.3, and log n = 3.9 ± 0.4 cm^{-3} for $N(CO)/dV = 1\times10^{17}$, 3×10^{17}, and 10×10^{17} cm^{-2}/ km s^{-1}, respectively.

When the implied mean temperature and density are relatively low, multiple gas components are required for good fits. This applies to about a third of the sample, characterized by a threshold of [C I] (2−1) ≈ 1.65. This corresponds roughly to mean values for kinetic temperature and density below 20 K and a few times 1000 cm^{-3}, respectively.

However, we conclude that the combined [C I] and ^{12}CO line ratios can generally be fit succesfully by a single (molecular) gas component above this threshold. In that case, the observed

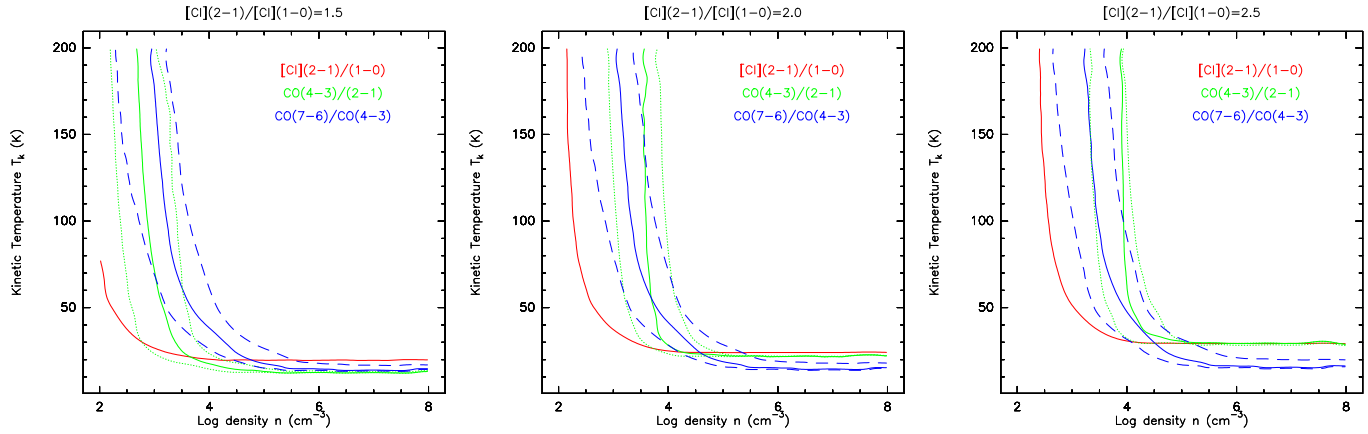

Fig. 5. LVG results for the [C I] and ^{12}CO line flux ratios observed in the galaxy sample. The panels contain lines of constant flux ratio, as a function of H_2 gas kinetic temperature T_k and volume density $n(H_2)$, for distinct C and CO column densities N/dV. *From left to right*: a. intersection of curves of constant line ratio [C I] (2−1)/(1−0) = 1.5 (≈20 K) and corresponding line ratios ^{12}CO (4−3)/^{12}CO (2−1) = 4.5 and ^{12}CO (7−6)/^{12}CO (4−3) = 0.9; b. intersection of curves of constant line ratio [C I] (2−1)/(1−0) = 2.0 (≈25 K) and corresponding line ratios ^{12}CO (4−3)/^{12}CO (2−1) = 6 and ^{12}CO (7−6)/^{12}CO (4−3) = 1.05; c. intersection of curves of constant line ratio [C I] (2−1)/(1−0) = 2.5 (≈30 K) and corresponding line ratios ^{12}CO (4−3)/^{12}CO (2−1) = 7 and ^{12}CO (7−6)/^{12}CO (4−3) = 1.35. In all three panels, CO curves are given for column densities N(CO)/dV = 1×10^{17} cm^{-2}/ km s^{-1}, (upper curve), 3×10^{17} cm^{-2}/ km s^{-1}, and 1×10^{18} cm^{-2}/ km s^{-1} (lower curve). Since the single [C I] (2−1)/(1−0) curve represents a column density N(CO)/dV = 1×10^{17} cm^{-2}/ km s^{-1}, the CO curves effectively correspond to [C]/[CO] abundances of 1, 0.3, and 0.1, respectively.

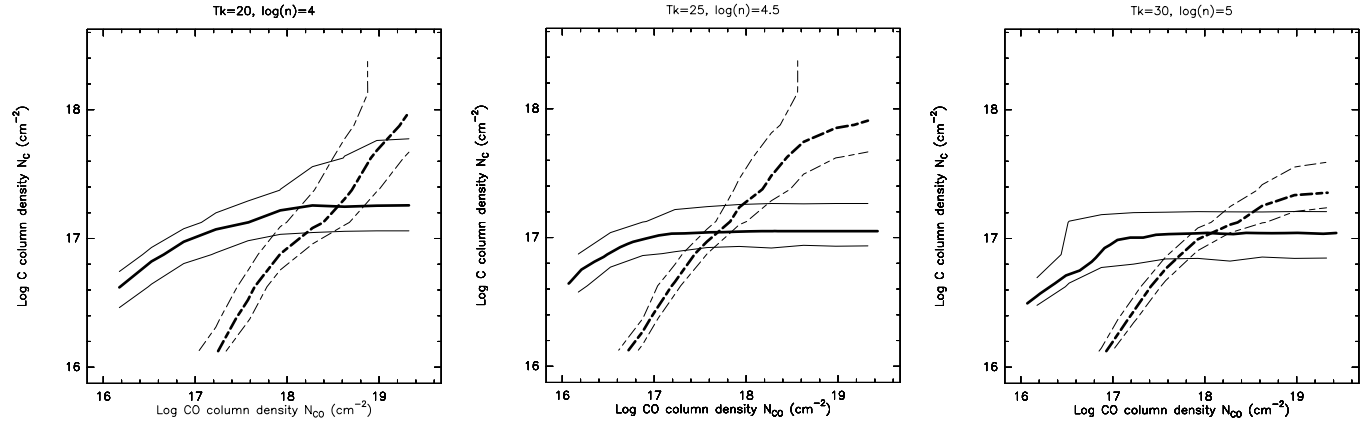

Fig. 6. LVG results for the [C I]-to-^{12}CO line flux ratios observed in the galaxy sample. The panels contain lines of constant flux ratio ^{12}CO (4−3)/[C I] (1−0) (solid lines) and ^{12}CO (7−6)/[C I] (2−1) (dashed lines) as a function of carbon and carbon monoxide column densities N_C/dV and N_{CO}/dV. *From left to right*: a. model curves at (T_k = 20 K, n = 10^4 cm^{-3}) for ratios ^{12}CO (4−3)/[C I] (1−0) = 1.1, 1.4, 2.0 and ^{12}CO (7−6)/[C I] (2−1) = 0.5, 0.8, 1.1; b. model curves at (T_k = 25 K, n = 3×10^4 cm^{-3}) for ratios ^{12}CO (4−3)/[C I] (1−0) = 1.4, 2.0, 2.6 and ^{12}CO (7−6)/[C I] (2−1) = 0.8, 1.1, 1.4; c. model curves at (T_k = 30 K, n = 10^5 cm^{-3}) for ratios ^{12}CO (4−3)/[C I] (1−0) = 2.0, 2.6, 3.2 and ^{12}CO (7−6)/[C I] (2−1) = 1.1, 1.4, 1.7. The diagram axes are column densities for a velocity interval of 1 km s^{-1}.

emission implies a gas of mean volume density log $n(H_2)$ = 4.7 ± 1.0 cm^{-3} and kinetic temperature ranging from T_k = 25 to 35 K. The limited range of solutions suggests that this is a robust conclusion. Moreover, with this result we can proceed to constrain the column densities N/dV and even the [C]/[CO] abundances.

4.4. [C I]/^{12}CO line ratios: the [C]/[CO] abundance

In Fig. 6 we plot the ratios of the two [C I] lines to their adjacent ^{12}CO line, ^{12}CO (4−3)/[C I] (1−0) and ^{12}CO (7−6)/[C I] (2−1) in the N_CdV–N_{CO}dV diagram, for a variety of temperature and density combinations corresponding to [C I](2−1)/(1−0) ratios of 1.5, 2, and 2.5. The intersections vary only a little as a function of conditions. The CO column densities are the same in all cases within a factor of two, and the C column densities are all within a factor of three from one another. The implied CO column densities do not vary much with circumstances, unlike the C column densities that drop a little with increasing temperature and density. Both decrease somewhat with increasing CO/C flux ratio, C more so than CO. The consistency of the results once more suggests that our assumption of ^{12}CO and [C I] emission originating in related gas clouds is correct. Summarizing these results, we find averaged column density gradients that characterizing the emission log N_{CO}/dV = 18.0 ± 0.3 cm^{-2}/ km s^{-1} and N_C/dV = 17.1 ± 0.5 cm^{-2}/ km s^{-1}. Individual (inverse) carbon abundance [CO]/[C] range from 3 to 20, but we find an averaged mean abundance [CO]/[C] = 8 ± 3. Thus, the amount of neutral carbon appears to be a rather small fraction of the amount of carbon monoxide. The results obtained so far thus indicate that the observed [CI] emission arises from a moderately dense (n, = 10^4–10^5 cm^{-3}) and warmish (T ≈ 30 K) gas, and representing only 10%–20% of the carbon in the gas phase.

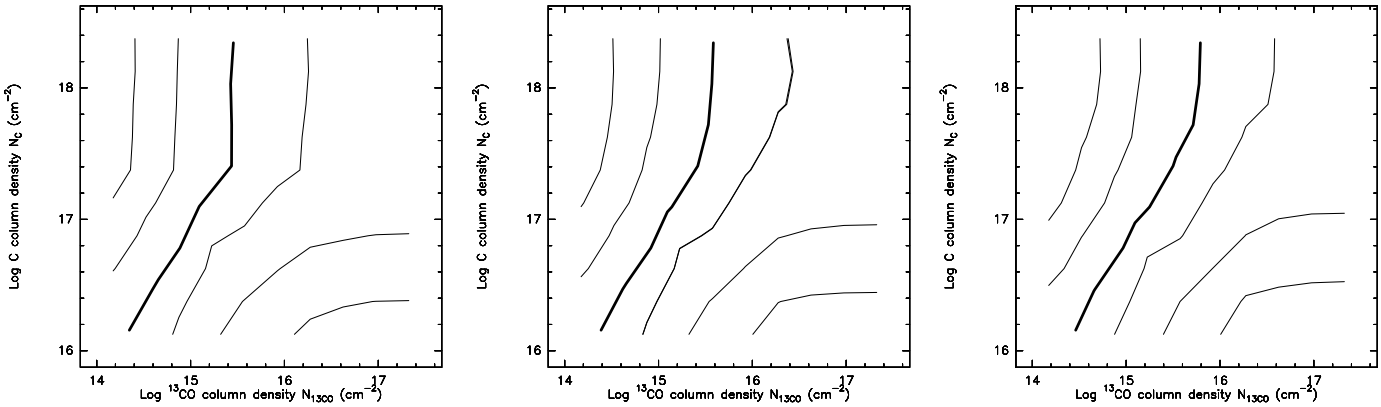

Fig. 7. LVG results for the [C I]-to-^{13}CO line flux ratios observed in the galaxy sample. The panels contain lines of constant flux ratio [C I] (1−0)/ ^{13}CO (2−1) as a function of carbon and carbon monoxide column densities N_C/dV and N_{13CO}/dV. *From left to right*: a. model curves at (T_k = 20 K, $n = 10^4$ cm^{-3}) for ratios [C I] (2−1)/(1−0) = 1, 3, 10, 30 (thick line), 100, and 300 increasing *from right to left*; b. as panel a., but for (T_k = 25 K, $n = 3\times10^4$ cm^{-3}); c. as panel a., but for (T_k = 30 K, $n = 10^5$ cm^{-3}). The diagram axes are column densities for a velocity interval of 1 km s^{-1}.

This is consistent with the results obtained by IB02, except for their conclusion that neutral carbon and carbon monoxide column densities are similar. The abundances found here are also lower than the range of 0.4−3.0 (mean value 1.2) that we have derived for a total of fifteen nearby galaxy centers from a more detailed analysis involving two gas phases (Israel 2009b, and references therein). It may be possible that a more detailed multiphase analysis of the luminous galaxies in the present sample would yield higher [C]/[CO] abundances.

4.5. [CI]/^{13}CO *line ratios: the* [C]/[^{13}CO] *abundance*

In Fig. 7 lines of constant [C I] (1−0)/ ^{13}CO (2−1) flux in the N_C/dV, N_{13CO}/dV diagram. As Fig. 1 shows, the sample galaxies have ratios between 10 (^{13}CO relatively strong) and 100 ([C I] that are relatively strong), with a mean at 30. The flux ratio [C I] (2-1/[C I] (1−0) that distinguishes the three panels of Fig. 7 appears to be uncorrelated with the [C I] (1−0)/ ^{13}CO (2−1) ratio, so that we expect the results of any analysis to be very similar for the three panels. This turns out to be the case. At the neutral carbon column densities N_C/dV determined in the previous section, Fig. 7 shows practically identical values log N_{13CO}/dV = 15.12±0.15, 15.06±0.13, and 15.12±0.17 for the mean observed line ratio of thirty. At the lowest observed line ratio of ten, galaxy centers have ^{13}CO column densities higher in the log by about 0.6: log $N_{13CO}/dV \approx 15.7$. Similarly, galaxies with very high [C I] (1−0)/ ^{13}CO (2−1 line ratios of a hundred have ^{13}CO column densities lower to the same degree: log $N_{13CO}/dV \approx 14.5$.

We performed the same analysis for the [C I] (2−1)/ ^{13}CO (2−1) line ratio (not shown) and find very similar column densities log $N_{13CO}/dV \approx 15.1$ for the mean sample galaxy, but tighter limits of Δ log N_{13CO}/dV = +0.4 and −0.2 on the galaxies with the highest and lowest line ratios, respectively. Although the LVG ^{13}CO column densities are fairly insensitive to changes in model temperature and density, they do increase by about a factor of two from galaxies with a low ^{12}CO/[C I] flux ratio to those with a high flux ratio in Fig. 6 and, of course, by a larger factor of 3 to 10 when going from galaxies with a high [C I]/ ^{13}CO ratio to those with a low ratio in Fig 7. Thus, the ^{13}CO model column densities of the sample galaxies are constrained to the range of N_{13CO}/dV = $1.25(+1.8, -0.7)\times10^{15}$ cm^{-3}/ km s^{-1}. Thus, Fig. 7 suggests that abundance ratio [[C I]]/[^{13}CO] ranges from about 25 (in galaxies with high CO/[C I] flux ratios) to about 250 (in galaxies with low CO/[C I] flux ratios).

5. Discussion

5.1. Importance of dense molecular gas in LIRG ISM

In the galaxies with the highest [C I] (2−1)/[C I] (1−0) and [C I] (1−0) / ^{13}CO (2−1) flux ratios, the ISM is fully dominated by dense (n(H_2) = 10^4−10^5 cm^{-3}) and modestly warm (T_{kin} = 20−35 K) gas. Low [C]/[CO] and very low [^{13}CO]/[^{12}CO] abundances of 0.1 and 0.01−0.001, respectively, further characterize this gas. This subsample is about two thirds of the total sample, and it contains all the (U)LIRGs in addition to fewer less luminous starburst galaxies. Thus, at least in the more luminous LIRGs, most of the interstellar gas is in the form of dense, warmish gas clouds. Diffuse molecular gas clouds of low density are probably also present, but not as important, contributors to the line emission from these galaxies.

This is no longer true if we consider galaxies with lower [C I] (2−1)/[C I]1−0) ≤ 1.65 and [C I] (1−0) / ^{13}CO (2−1) ≤ 30 ratios. In these galaxies, the assumption of a single high-pressure gas phase still yields good fits to the individual observed line ratios, but the physical parameters derived from these fits become increasingly inconsistent as we go to ever lower [C I] (2−1)/[C I] (1−0) and [C I] (1−0)/ ^{13}CO (2−1) ratios. For instance, we no longer can obtain consistent results for density and temperature at observed ratios [C I] (2−1)/[C I] (1-0) ≤ 1.5. Moreover, a succesful combination of the results of Sects. 4.3 and 4.4 is only possible if the isotopic ratios are very high [^{12}CO]/[^{13}CO] = 200−3000 (median value 400). Such values are much higher than the isotopic ratios in the Milky Way, which are typically 25 to 100 (see, for instance, Giannetti et al. 2014, and references therein). As already noted, high ^{12}CO/ ^{13}CO ratios have been found before in starburst galaxies (Martín et al. 2010; Henkel et al. 2014), but their values are not nearly as high as the ones we find here. Even worse, such very high [^{13}CO]/[^{12}CO] abundances are actually irreconcilable with observed J = 2−1 isotopic flux ratios, and the model also predicts J = (1−0) isotopic flux ratios to be higher than those in the J = 2−1 transition by factors of two to three times, which is contradicted by observation (see, e.g., Papadopoulos et al. 2012; and Davis 2014).

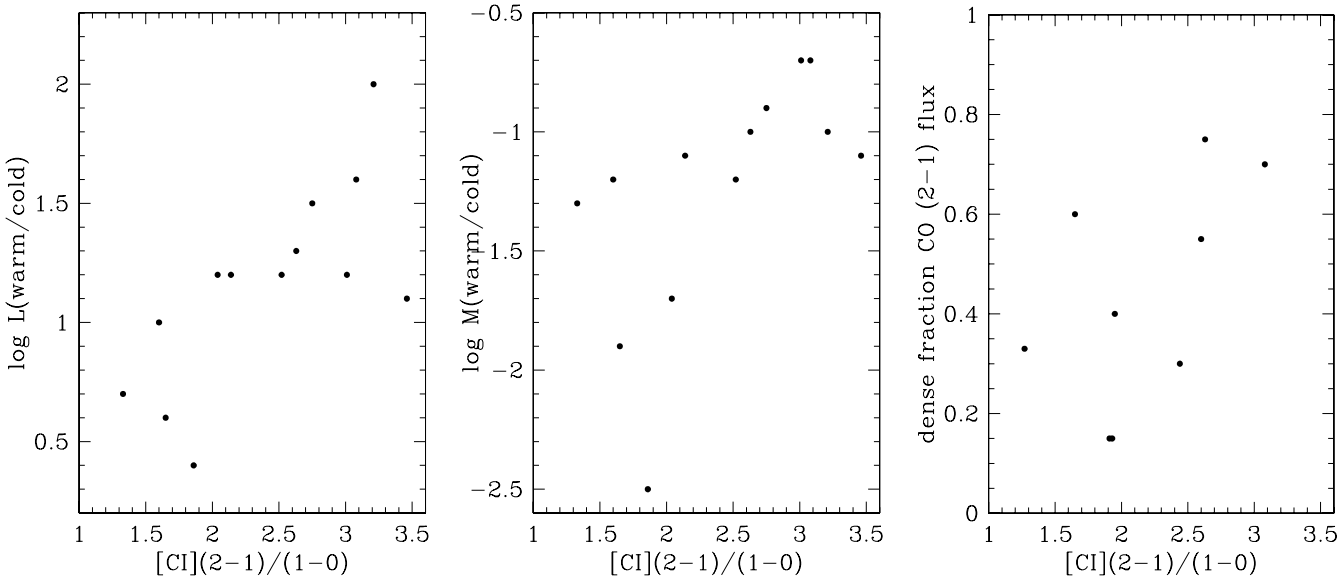

Fig. 8. Diagnostic two-phase gas ratios as a function of the observed [C I] (2−1)/(1−0) line flux ratio. The *left panel* shows the behavior of the 'warm/cold/ratio of total CO line luminosities, taken from Kamenetzky et al. (2014) versus the [C I] line ratio from this paper. The *center panel* shows the corresponding "warm/cold" ratio of molecular gas masses. The *right panel* shows the fraction of the ^{12}CO $J = 2-1$ flux that is ascribed to "dense" gas, based on the results published by Israel (2009b, and references therein). All three quantities increase in favor of "warm" and "dense" with increasing [C I] line flux ratio.

Thus, our assumption that the [C I] and ^{12}CO line emission is characterized by a single temperature and a single density breaks down in galaxies with decreasing [C I] (1−0)/ ^{13}CO (2−1) and [C I] (2−1)/(1−0) flux ratios. Galaxies with FIR luminosities log L(FIR) $\geq$ 11.3 can all be fit with a single gas component. For starburst galaxies with 10.3 $\leq$ L(FIR) $\leq$ 11.3 this is true for 60%, and for those with L(FIR) $\leq$ 10.3 this has dropped to 45%. Although there is no distinct luminosity threshold, the lower the luminosity of a galaxy, the greater the chance that it requires modeling with at least two gas phases. Dense gas ($n(\mathrm{H_2}) \geq 10^4$ cm^{-3}) is still in evidence, but the contribution of gas at lower densities and temperatures, i.e. at lower pressures, becomes increasingly important and can no longer be ignored. Assigning part of the observed line emission to a contribution by low-excitation gas, we might increase the total mass significantly beyond the mass estimated from the single-phase analysis; for this reason, we have refrained from attempting to estimate masses in the preceding sections.

However, such a two-phase LVG analysis has recently been performed and published by Kamenetzky et al. (2014, hereafter K14). Their sample is a small subset (15 out of 76 galaxies) of the sample in this paper, which nevertheless covers the full range of FIR luminosities. They also include two (early type) galaxies that we ignore in the following. In their analysis, K14 likewise relied on RADEX to fit all the ^{12}CO lines up to J = 13−12, and modeled dust, mid-infrared H_2 lines, and the [C I], [C II], and [N II] fine-structure lines as well, but they did not include any ^{13}CO fluxes. To obtain masses, they assumed an abundance $[\mathrm{CO}]/[\mathrm{H_2}] = 2 \times 10^{-4}$ throughout. Since K14 used the same data and the same non-LTE code to analyze the data, their results should be comparable to ours. Their [C I] LTE excitation temperatures (their Table 14) indeed lie in the same range as our non-LTE kinetic temperatures. K14 distinguish between a "cold" and a "warm" gas phase contribution to the observed line emission and derive the parameters for each of these. The cold and warm CO phases have similar densities, on average $n(\mathrm{H_2})$ = 2000 cm^{-3} (range 200−25 000 cm^{-3}) and $n(\mathrm{H_2})$ = 7000 cm^{-3} (range 1000−75 000 cm^{-3}), respectively, but the temperatures are very different, T_{kin} = 25 K (range 15−250 K) for the cold phase and 725 K (range 250−2500 K) for the warm phase. The CO column densities they find are very similar to our values for the cold phase and an order of magnitude lower than what we find for the warm component. Thus, the more complicated two-phase modeling by K14 that provides a better fit to (a subset of) the data in this paper still yields physical results that are not very different from those derived from our simplified one-phase fits.

The K14 analysis yields molecular gas masses for both "warm" and "cold" gas phases, as well as their pressures and the luminosity of the total CO line luminosity. In the above, we concluded that the contribution from dense gas increasingly dominates the observed line fluxes for increasing [C I] (1−0)/(2−1) ratios. Thus, at the higher [C I] ratios, the "warm" component should also increasingly dominate the "cold" component in the K14 results. In Fig. 8, we show both the CO luminosity ratio and the gas mass ratio of the warm and cold phases distinguished by K14 (taken from their Table 13), as a function of the [C I] line ratio. Eight of the galaxies in our sample have also been mapped and studied in more detail before (Israel 2009b, and references therein), likewise involving a two-phase LVG analysis based on RADEX. For these eight galaxies, we took the fraction of the total ^{12}CO (2−1) flux that the models require to be attributable to the dense gas phase. Although the small numbers and the relatively large dispersions of the data in each panel, as well as differences in method and lines considered, rule out a fruitful quantitative comparison between the panels and the results obtained in the above, all three panels nevertheless show the qualitative behavior that is expected if the role of dense gas is indeed more dominant at the higher [C I] (2−1)/(1−0) ratios.

5.2. Use of [C$_{\mathrm{I}}$] as a tracer of molecular gas

Because cold H_2 gas is very hard to observe, its surface density and mass are usually estimated from measurements of dust or tracer molecules. The ubiquitous CO molecule is such a

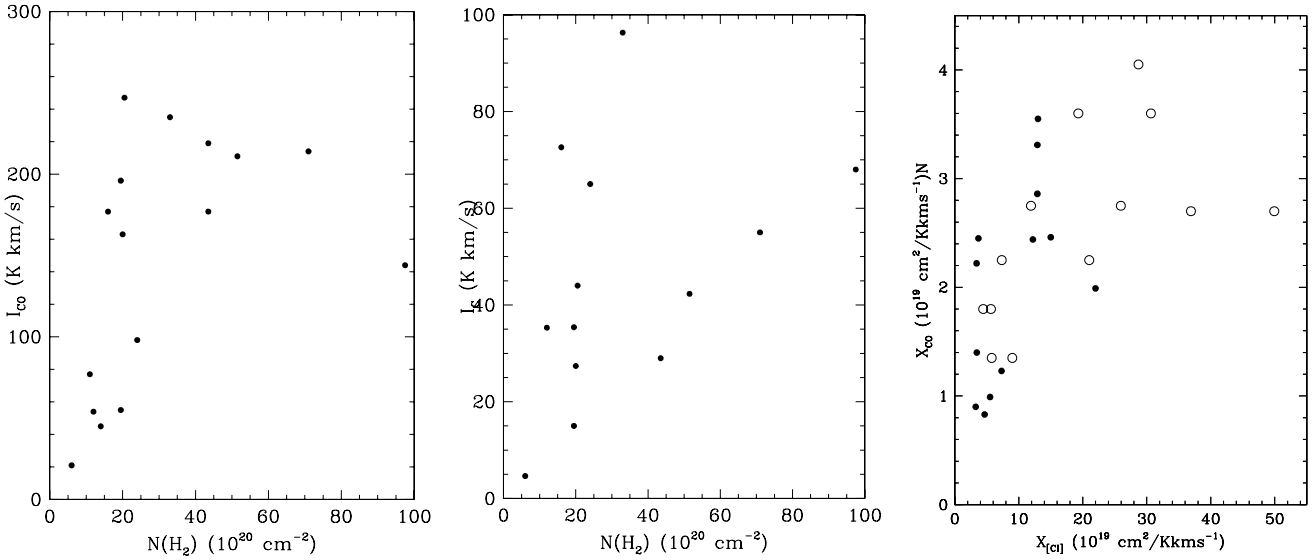

Fig. 9. Comparison of $N_{H_2}/I_{[CI]}$ and N_{H_2}/I_{CO} conversion factors based on the [C I] (1−0) and ^{12}CO (1−0) emission from fully modeled galaxy centers (see text). The open circles in the rightmost panel represent data extracted from the study by Kamenetzky et al. (2014).

tracer, even though the ^{12}CO lines are optically thick, have metallicity-dependent abundances, and are subject to various excitation conditions that in the worst case lead to its dissociation. Nevertheless, the beam-averaged ^{12}CO (1−0) intensity is often used to derive H_2 column densities on the assumption that variations in the actual ratio of ^{12}CO intensity to H_2 column density across the (large) linear beam area cancel out, so that a common factor (called X_{CO}) can be used to perform the conversion. The actual value of X_{CO} to be used and the ways in which it varies as a function of environmental conditions are still under debate (see, for instance, the review by Bolatto et al. 2013).

It has been suggested by various authors (Papadopoulos et al. 2004; and more recently Offner et al. 2014; Glover et al. 2015; and Tomassetti et al. 2014) that [C I] line intensities may be a better tracer of line-of-sight molecular hydrogen gas column densities than either ^{12}CO or ^{13}CO, especially the 492 GHz ^{12}CO $J = 1-0$ transition that is easiest to observe. Their conclusions are supported by model simulations of spatially resolved Galactic clouds. An important consideration is that they expect neutral carbon to be widespread and thoroughly mixed with turbulent molecular gas in filamentary clouds and that it traces diffuse gas of lower densities than ^{12}CO and ^{13}CO. Tomassetti et al. (2014) even claim that spatially unresolved [C I] measurements may recover the entire H_2 mass of a galaxy (but the kinetic temperature and the neutral carbon abundance need to be known first).

In the preceding we have found, however, that much or even most of the [C I] emission traces dense $n(H_2) \geq 10^4$ cm^{-3} clouds rather than a diffuse gas, and that conditions may vary considerably as a function of excitation. This appears to be at odds with one of the major assumptions underlying the case for [C I] emission as a superior or even useful tracer of molecular gas. It is thus of interest to compare [C I]-to-H_2 conversion factors to the more traditional CO-to-H_2 conversion factor using actual observations of unresolved cloud ensembles. We have done this by determining the ratios $X_C = N_{H_2}/I([CI]_{492})$ and $X_{CO} = N_{H_2}/I(CO_{115})$ for fifteen galaxy centers modeled using ground-based observations (see Israel 2009b, and references therein). For these galaxies, beam-averaged column densities N_{H_2} were derived from the lower ^{12}CO and ^{13}CO transitions, assuming a mixture of two gas phases (a warm low-density phase and a colder high-density phase). Although physically not fully realistic, these two-phase LVG models are clearly superior to the single-phase LVG model considered thus far.

The results are shown in Fig. 9. We find mean values $X_{CO} = (0.21 \pm 0.10) \times 10^{20}$ cm^{-2}/ K kms^{-1}, and $X_C = (1.0 \pm 0.6) \times 10^{20}$ cm^{-2}/ K kms^{-1}. The mean CO-to-H_2 conversion factor derived from this sample is very close to the mean values found in the two-phase analysis by K14 and suggested earlier by Papadopoulos et al. (2012) and Yao et al. (2003). This mean value of X_{CO} is a full order of magnitude lower than the value usually assumed for galaxy disks (the "standard" conversion factor), and a factor of two or more below the value often applied instead to active galaxy centers.

The good agreement between the mean X values quoted hides the fact, however, that neither the individual velocity-integrated ^{12}CO fluxes nor the individual [C I] fluxes correlate very well with the derived beam-averaged H_2 column densities as shown in the lefthand and center panels of Fig. 9. In the rightmost one, we also compare directly the X_{CO} and X_C values, derived from the preceding work. In that panel, we have also included X values deduced from K14. Overall, the two are roughly correlated but show significant variations from galaxy to galaxy over a range that covers an order of magnitude.

We conclude that in practice the [C I] 492 GHz line is not superior to the ^{12}CO 115 GHz line as a tracer of molecular (H_2) gas. Even though the data indicate mean conversion factors about an order of magnitude lower than the "standard" Galactic values, there appear to be no a priori reliable [C I]-to-H_2 or CO-to-H_2 conversion factors that can be used to find the masses of individual galaxy centers or luminous galaxies in general. It is therefore quite likely that the [C II] line at 1.9 THz, not studied in this paper, is superior to both CO and [C I] as a molecular gas tracer, and it is also conceivable that variations in environmental conditions require analysis of all three lines together to arrive at reliable estimates.

The above considerations reinforce our conviciction that an attempt to use the results of a simple analysis such as provided here to derive the total mass of molecular gas in the observed galaxy centers would be a meaningless, even misleading exercise.

5.3. Molecular gas in high-redshift galaxies

Our findings have some relevance for the study of the molecular content of luminous galaxies in the early Universe. Especially with millimeter array telescopes, measurements of individual CO and [CI] lines have become quite feasible, but these are frequently difficult to interpret. Standard CO-to-H_2 conversion factors (although sometimes applied) are utterly useless, because the physical circumstances in luminous high-z galaxies are not really known and are certainly different from the local circumstances on which such factors are based. In fact, this is what we actually want to determine. In any case, the X-factor only (if at all) applies to the $J = 1-0$ transition of CO, which is rarely observed. By themselves, high CO transitions ($J > 5$) sample a limited fraction of the molecular gas, and FIR dust temperatures often do not usefully constrain the kinetic gas temperatures. As illustrated in earlier sections of this paper, ^{12}CO line ratios are highly degenerate for temperature and density. Emission in one of the ^{13}CO lines, which might be used to break this degeneracy, are almost always lacking, owing to their intrinsic weakness (cf. Fig. 2d).

The method we have applied to luminous galaxies in the local Universe, however, might also be used to determine parameters for their early Universe counterparts. If we can measure the three ^{12}CO lines, as well as the two [C I] lines for these galaxies, we may also determine the intersection of their ratios, hence their density and kinetic temperature of the underlying H_2 gas, and the C and CO average column densities.

Unfortunately, the opacity of the (sub)millimeter sky does not allow measurement of these lines at all redshifts of interest. However, in addition to the local Universe, all five lines occur in atmospheric windows for the following redshift ranges: $z1 = 0.15-0.18$, $z2 = 0.9-1.1$, $z3 = 1.2-1.4$, $z4 = 1.8-2.2$, $z5 = 3.1-3.2$, and $z6 = 3.7-5.2$. Line ratios of objects in any of these redshift ranges can be analyzed immediately using RADEX-derived diagnostic diagrams of the type presented in this paper. In principle, such ratios need to be corrected for the change in cosmic background temperature T_{bg} that increases from 3.2 K at z1 to >13 K at z6. These corrections are not large. For the gas parameters of the average luminous galaxy in this paper, the CO(4−3)/CO(2−1) ratio increases up to z6 by no more than 10%, and the CO(7−6)/(4−3) ratio increases by less than 20%. The increases in the [C I] and in the [C I]-to-^{12}CO ratios are likewise less than 10% so that even uncorrected use of the diagrams in Figs. 4–6 produces useful results.

6. Conclusions

We collected flux measurements of the two lines of neutral carbon [C I] at 492 GHz and 809 GHz from 76 galaxies, mostly obtained with the SPIRE instrument on the *Herschel* Space Observatory, as well as the fluxes of the $J = 7-6$, $J = 4-3$, $J = 2-1$ ^{12}CO, and $J = 2-1$ ^{13}CO lines. In 35 galaxies, all six lines have been measured.

In most galaxies or galaxy centers observed, the ratio of the [C I] to ^{13}CO line flux is much higher than the corresponding ratio in Galactic sources. The ratio increases with both line and FIR continuum luminosity, and this both confirms and expands an earlier conclusion using data from ground-based facilities alone. The flux ratio of the two [C I] lines correlates well with both the $J = 7-6/J = 4-3$ and the $J = 4-3/J = 2-1$ flux ratios of ^{12}CO; higher [C I] and ^{12}CO ratios trace more highly excited molecular gas.

The observed [C I] lines alone do not provide much quantitative information on the conditions in the ISM of the parent galaxies, because their flux ratio is highly degenerate with respect to density and temperature. However, when combined with ^{12}CO line ratios, the [C I] lines do significantly constrain the ISM parameters and provide a useful criterion to classify the parent galaxies in terms of ISM gas pressure. The galaxies with the highest [C I] flux ratios and the highest [C I]/^{13}CO flux ratios represent the warmest and most luminous galaxies, classified as Luminous InfraRed Galaxies (LIRGs). Their emission is reproduced well by single-gas-phase LVG models.

The ISM in the most luminous LIRGs, as traced by the observed line emission, is fully dominated by dense ($n(H_2) = 10^4-10^5$ cm^{-3}) and moderately warm ($T_{kin} \approx 35$ K) gas clouds. They appear to have low [C°]/[CO] and [^{13}CO]/[^{12}CO] abundance ratios. In the more numerous, less luminous galaxies, a single gas-phase LVG model no longer produces consistent results. In these galaxies, emission from gas clouds at lower densities becomes progressively more important in addition to the emission from dense clouds, and a multiple-phase analysis is required.

This analysis shows that both ^{12}CO and [C I] velocity-integrated line fluxes poorly predict molecular hydrogen (H_2) column densities in the high-excitation environments exemplified by (active) galaxy centers and the ISM of luminous infrared galaxies. In particular, so-called X([C I]) conversion factors do not outperform X(^{12}CO) factors.

The methods and diagnostic diagrams presented in this paper also provide a means of deriving temperatures, densities, and column densities of the molecular gas in high-redshift galaxies, from ^{12}CO and [C I] lines alone. We have identified six redshift ranges for which all five lines required fall in windows of good sky transparency.

References

Aalto, S., Booth, R. S., Black J. H., & Johansson, L. E. B. 1995, A&A, 300, 369
Albrecht, M., Krügel, E., & Chini, R. 2007, A&A, 462, 575
Bayet, E., Gerin, M., Phillips, T. G., & Contursi, A. 2006, A&A, 460, 467
Bolatto, A. D., Wolfire, M., & Leroy, A. K. 2013, ARA&A, 51, 207
Bridges, T. J., & Irwin, J. A. 1998, MNRAS, 300, 967
Davis, T. A. 2014, MNRAS, 445, 2378
Fixsen, D. J., Bennett, C. L., & Mather, J. C. 1999, ApJ, 526, 207
Gerin, M., & Phillips, T. G. 2000, ApJ, 537, 644
Giannetti, A., Wyrowski, F., Brand, J., et al. 2014, A&A, 570, A65
Glover, S. C. O., Clark, P. C., Micic, M., & Molina, F. 2015, MNRAS, 448, 1607
Griffin, M. J., Abergel, A., Abreu, A., et al. 2010, A&A, 518, L3
Henkel, C., Asiri, H., Ao, Y., et al. 2014, A&A, 565, A3
Hitschfeld, M., Aravena, M., Kramer, C., et al. 2008, A&A, 479, 75
Hogerheijde, M. R., & van der Tak, F. F. S. 2000, A&A, 362, 697
Israel, F. P. 2009a, A&A, 506, 689
Israel, F. P. 2009b, A&A, 493, 525
Israel, F. P., & Baas, F. 2001, A&A, 371, 433
Israel, F. P., & Baas, F. 2002, A&A, 383, 82 (IB02)
Israel, F. P., & Baas, F. 2003, A&A, 495, 504
Israel, F. P., White, G. J., & Baas F. 1995, A&A, 302, 343
Israel, F. P., Tilanus, R. P. J., & Baas F. 2006, A&A, 445, 907
Israel, F. P., Güsten, R., Meijerink, R., et al. 2014, A&A, 562, A96
Jansen, D. J. 1995, Ph.D. Thesis, University of Leiden (NL)
Jansen, D. J., van Dishoeck, E. F., & Black, J. H. 1994, A&A, 282, 605
Kamenetzky, J., Rangwala, N., Glenn, J., Maloney, P. R., & Conley, A. 2014, ApJ, 795, 174
Kaufman, M. J., Wolfire, M. G., Hollenbach, D. J., & Luhman, M. L. 1999, ApJ, 527, 795
Kazandjian, M. V., Meijerink, R., Pelupessy, I., Israel, F. P., & Spaans, M. 2012, A&A, 542, A65
Martín, S., Aladro, R., Martín-Pintado, J., & Mauersberger, R. 2010, A&A, 522, A62
Meijerink, R., & Spaans, M. 2005, A&A, 436, 397
Meijerink, R., Spaans, M., & Israel, F. P. 2007, A&A, 461, 793

Offner, S., Bisbas, T. G., Bell, T. A., & Viti, S. 2014, MNRAS, 440, L81
Panuzzo, P., Rangwala, N., Rykala, A., et al. 2010, A&A, 518, L37
Papadopoulos, P. P., Thi, W.-F., & Viti, S. 2004, MNRAS, 351, 147
Papadopoulos, P. P., van der Werf, P. P., Xilouris, E. M., et al. 2012, MNRAS, 426, 2601
Papadopoulos, P. P., Zhang, Z.-Y., Xilouris, E. M., et al. 2014, ApJ, 788, 153
Pereira-Santaella, M., Spinoglio, L., Busquet, G., et al. 2013, ApJ, 768, 55
Pereira-Santaella, M., Spinoglio, L., van der Werf, P. P., & Piqeras López, J. 2014, A&A, 566, A49
Pilbratt, G. L., Riedinger, J. R., Passvogel, T., et al. 2010, A&A, 518, L1
Plume, R., Jaffe, D. T., Tatematsu, K., Evans, N. J., & Keene, J. 1999 ApJ, 512, 768
Rosenberg, M. J. F., Kazandjian, M. V., van der Werf, P. P., et al. 2014a, A&A, 564, A126
Rosenberg, M. J. F., Meijerink, R., Israel, F. P., et al. 2014b, A&A, 568, A90
Rosenberg, M. J. F., van der Werf, P. P., Aalto, S., et al. 2015, ApJ, 801, 72
Sakamoto, K., Ho, P. T. P., & Perk, A. B. 2006, ApJ, 644, 862
Schirm, M. R. P., Wilson, C. D., Parkin, T. J., et al. 2014, ApJ, 781, 101
Sliwa, K., Wilson, C. D., Petitpas, G. R., et al. 2012, ApJ, 753, 46
Spinoglio, L., Pereira-Santaella, M., Busquet, G., et al. 2012, ApJ, 758, 108
Tatematsu, K., Jaffe, D. T., Plume, R., Evans, N. J., & Keene, J. 1999, ApJ, 526, 295
Tomassetti, M., Porciani, C., Romamo-Diaz, E., Ludlow, A. D., & Papadopoulos, P. P. 2014, MNRAS, 445, L124
Ueda, J., Iono, D., Yun, M. S., et al. 2014, ApJS, 214, 1
Walter, F., Weisz, A., Downes, D., Decarli, R., & Henkel, C. 2011, ApJ, 730, 18
Ward, J. S., Zmuidzinas, J., Harris, A. I., & Isaak, K. G. 2003, ApJ, 587, 171
Yao, L., Seaquist, E. R., Kuno, N., & Dunne, L. 2003, ApJ, 588, 771
Zhang, Z.-Y., Henkel, C., Gao, Y., et al. 2014, A&A, 568, A122